SPE Canadian Energy Technology Conference and Exhibition held 13-14 March 2024 in Calgary, Alberta, Canada.

SPE-218077-MS

A Study Of DME-steam Co-injection Using A Large-scale Physical Model

H. Amer[1], K. Sheng[1], R. Okuno[1], A. Filstein[2], M. French[2], J. Sanchez[3], A. Al-Gawfi[4], and P. Nakutnyy[4]

[1]Hildebrand Department of Petroleum and Geosystems Engineering, University of Texas at Austin, Austin, Texas, USA
[2]ConocoPhillips, Calgary, Alberta, Canada
[3]ConocoPhillips, Doha, Qatar
[4]Saskatchewan Research Council, Regina, Saskatchewan, Canada

Abstract

Dimethyl ether (DME) as a water-soluble solvent has been studied as a potential additive to steam for improving the energy efficiency of steam-assisted gravity drainage (SAGD). The main objective of this research was to study in-situ flow characteristics and energy efficiency of DME-SAGD using a large-scale physical model. Results from DME-SAGD were compared with the control experiment of SAGD with no solvent injection using the same experimental setup. The main novelty of this research lies in the experimental data that demonstrated enhanced bitumen drainage by DME-SAGD in comparison to SAGD.

The experiment was conducted in a cylindrical pressure vessel with a diameter of 0.425 m and a length of 1.22 m, which contained a sand pack with a porosity of 0.34 and a permeability of 5.0 D. The DME-SAGD experiment used a DME concentration of 10 mol% and a steam co-injection rate of 27.6 cm^3/min [cold-water equivalent (CWE)] at 3000 kPa. Temperature distributions within the sand pack, along with injection and production histories, were recorded during the experiment. Subsequently, numerical simulations were performed to history-match the experimental data, and the calibrated simulation model was used to analyze details of compositional flow characteristics.

Results showed that the 10 mol% DME-SAGD experiment yielded a recovery factor of 92.7% in 4.2 days, and the SAGD experiment yielded a recovery factor of 68.6% in 6.0 days, for both of which the first 2 days were the preheating and the steam-only injection (SAGD) stages. The peak rate of bitumen production was 43.8 mL/min in the DME-SAGD experiment, which was more than twice greater than the peak rates observed in the SAGD experiment. The substantially increased rate of bitumen production resulted in a cumulative steam-to-oil ratio in DME-SAGD that was less than half of that in SAGD.

Analysis of experimental results indicated that the solubility of DME in the aqueous and oleic phases caused different flow characteristics between DME-SAGD and SAGD. For example, the oleic and aqueous phases were more uniformly distributed in the sand pack in the former. Simulations indicated that DME-SAGD had a uniform distribution of greater grid-scale Bond numbers and increased oleic-phase mobilities in comparison to SAGD.

Introduction

In-situ recovery methods for bitumen require increasing the in-situ oil mobility since viscosities of bitumen often exceed one million centipoises at standard conditions. Steam-assisted gravity drainage (SAGD) has been successfully applied to produce bitumen at the commercial scale (Butler 1981). SAGD involves the injection of steam into a top horizontal well, leading to the development and expansion of a steam chamber within the bitumen reservoir. The injected steam releases its latent heat upon condensation near the steam-chamber edge to the surrounding bitumen-bearing rock. Although only a fraction of the heat is used for heating the in-situ bitumen, the bitumen viscosity is quite sensitive to temperature. As a result, the heated bitumen becomes mobile and flows with the condensed water under gravitational forces. They are produced through a bottom horizontal well, typically positioned five meters below the injector. Later, Nasr et al. (2003) introduced expanding-solvent SAGD (ES-SAGD), which aimed to improve bitumen production rates, decrease the steam-to-oil ratio, and lower energy and water requirements in comparison to SAGD. Solvent-aided SAGD (SA-SAGD), including ES-SAGD, can enhance bitumen drainage through a combination of heating and dilution (or mixing) of in-situ bitumen. This research focuses on the use of dimethyl ether (DME) as a water-soluble solvent in SA-SAGD.

DME is the simplest ether with a chemical formula of C_2H_6O. It is a colorless and non-carcinogenic gas at standard conditions. DME's vapor pressure is between propane and n-butane at a given temperature. DME serves as an alternative fuel for powering turbines and engines (Fleisch et al. 1997; Semelsberger et al. 2006). There are different methods of DME synthesis, either from methanol or from syngas (Xu et al. 1997; Ng et al. 1999). The slight polarity makes DME partially soluble in water, but DME is first-contact miscible with oil.

Shell pioneered the application of DME in enhanced oil recovery, DME-enhanced waterflooding (DEW), which leverages DME's mutual solubility in aqueous (W) and oleic (L) phases. Several experimental and numerical studies revealed that the primary mechanisms in DEW are oil swelling and viscosity reduction (Chernetsky et al. 2015; Parsons et al. 2016; Mahdizadeh et al. 2019; Javanmard et al. 2019). The phase behavior of brine-DME-oil mixtures is crucial in determining DME's partitioning into these phases. Experimental data on DME-water and DME-hydrocarbon binary mixtures presented such partitioning behavior (Pozo and Streett 1984; Holldorff and

Knapp 1988; deFernández et al. 1992). Ratnakar et al. (2016a) matched phase behavior data for DME-brine-oil using a cubic-plus-association equation-of-state (EOS) based on the Soave-Redlich-Kwong model (1972). Subsequently, Ratnakar et al. (2016b) employed Huron and Vidal (HV) mixing rules (1979) for the Peng-Robinson EOS (1978) to match partitioning coefficient data of DME in the L and W phases. Using HV mixing rules was more convenient because they can be adapted in commercial reservoir simulators.

The first publications on DME as a steam additive for enhanced bitumen drainage are Sheng et al. (2017) and Okuno (2018). The simulation studies presented by Sheng et al. (2018) compared 2 mol% DME-SAGD with C_4-SAGD, in which DME-SAGD reduced gravity segregation between the W and L phases because of DME's mutual solubility, and achieved greater solvent recovery in comparison to C_4-SAGD. Haddadnia et al. (2018a) showed that bitumen drainage was similar for DME-SAGD and C_4-SAGD, with a 5-vol% solvent co-injected with steam at 1000 kPa in a 2D sand pack. Baek et al. (2019) measured viscosities for DME-bitumen mixtures and n-hexane-bitumen mixtures at different solvent concentrations. Their results showed that the two solvents had similar bitumen-dilution capability at temperatures above 107°C. Chai et al. (2023) carried out field-scale numerical simulations and showed that DME-SAGD was more effective in enhancing bitumen recovery in comparison to SAGD. They also concluded that the optimal concentration of DME co-injection ranged from 5 to 10 mol%. Amer et al. (2024b) compared 10 mol% DME-SAGD, 20 mol% C_4-SAGD, and SAGD at 3500 kPa using a small-scale physical model. Their experimental setup and procedures were designed to control thermodynamic conditions (i.e., temperature, pressure, and composition) at the vapor-chamber edge, as also presented by Sheng et al. (2022a) and Amer et al. (2024a). The results showed that 10 mol% DME-SAGD enhanced bitumen gravity drainage rate by 15% in comparison to 20 mol% C_4-SAGD. DME was also studied for warm VAPEX without steam injection with promising oil recovery results (Yang et al. 2021; Chai et al. 2022).

The previous studies referenced above suggested potential mechanisms of DME-SAGD for improving the energy efficiency of SAGD. The most fundamental cause for the proposed mechanisms comes from the slight polarity of DME that makes DME slightly soluble in water. The phase behavior in the presence of bitumen and water is the main difference between DME and hydrocarbon solvents as an additive to steam for SAGD. For example, DME-SAGD is expected to yield a higher temperature near the chamber edge (T_{edge}) than C_4-SAGD although DME and n-C_4 have similar volatility. This feature of DME-SAGD was originally predicted by Sheng et al. (2017) and Okuno (2018) and later experimentally observed by Amer et al. (2024b). Then, Baek et al. (2019) experimentally confirmed that DME and n-hexane were comparable as diluent for the same bitumen at their respective T_{edge}. Another expected mechanism is that DME-SAGD yields markedly different flow characteristics than SA-SAGD with hydrocarbon solvents; for example, the DME partitioning into the W and L phases ahead of the chamber edge is expected to enhance the mass transfer of DME into the bitumen-rich L phase and also to suppress the level of gravity segregation between the two liquid phases. Such flow characteristics of DME-SAGD were originally proposed in the numerical studies by Sheng et al. (2017) and Okuno (2018). Li et al. (2023) concluded that the density difference between the L and W phases was reduced at the steam-chamber edge with their 2-D DME-SAGD experiments. Recently, Amer et al. (2024b) showed such flow regimes with a distribution of greater Bond numbers in the sandpack, indicating the proposed mechanisms at play. **Figure 1** shows a schematic of DME-SAGD. The inter- and intra-mass transfer of DME in the L and W phases enhances the mixing of DME with bitumen within the solvent-bitumen mixing zone ahead of the steam-chamber edge in the ξ direction.

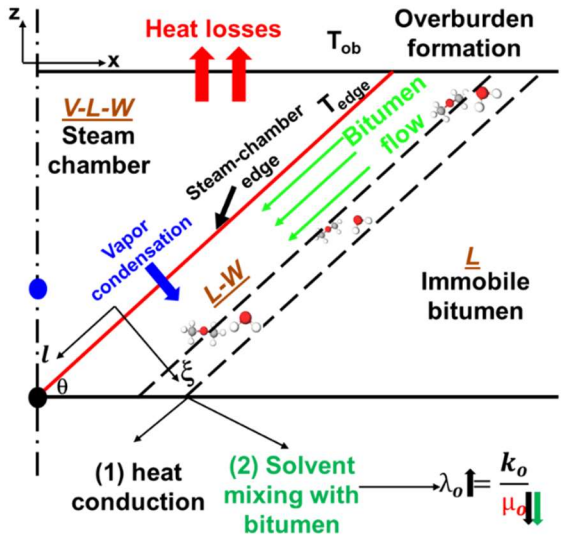

Fig. 1—A schematic diagram depicting bitumen gravity drainage in DME-SAGD (Amer et al. 2024b). The bitumen mobility is increased by heat and dilution in the mixing zone.

This paper presents experimental results of DME-SAGD and SAGD using a large-scale physical model and a detailed analysis of the experimental data using numerical simulation for in-situ thermal/compositional flow and energy efficiency. The DME-SAGD experiment used a DME concentration of 10 mol% in the injection stream, and was compared with SAGD with no solvent co-injection (the concentration is omitted to indicate the 10-mol% DME-SAGD experiment as "DME-SAGD" throughout the paper). Unlike Amer et al. (2024b), the large-scale experiment in this research enabled the investigation of DME-SAGD under transient conditions for the

steam-vapor chamber. In the following sections, the experimental method and results are presented first. Following this, the simulation history-matching procedure, results, and analysis are discussed. Finally, the main conclusions are summarized.

Experimental Methods

This section outlines the 3-D cylindrical experimental setup, the properties of the bitumen used, and the model packing and saturation procedures. It further provides details of the SAGD and DME-SAGD experiments, including preheating, steam (or DME/steam) injection, pressure depletion, produced fluid handling, and post-run excavation of the sand pack. The experimental procedure in this research is similar to that of Sheng et al. (2021 and 2022b) for SAGD and 2.8 mol% condensate-SAGD experiments.

Experimental Setup

Figure 2 presents a schematic of the experimental setup at Saskatchewan Research Council (SRC) used for this research. The main components of the setup included the following:

- A 1.22-meter-long carbon-steel cylindrical vessel with an outer diameter of 0.46 meters. The maximum operating temperature and pressure were 250˚C and 7000 kPa, respectively.
- Dual carbon steel flanges, designed to accommodate two horizontal wells—for injection and production—as well as a grid of thermocouples (TCs).
- Two centralized inline heaters, each 1.22 m in length, encircling both the injector and the producer. These heaters were integrated with TCs for real-time temperature readings. Specifically, the producer inline housed five TCs, while the injector inline contained three.
- Nineteen 5-point thermocouple lines, each spanning the entire model length of 1.22 m; hence, it consisted of 95 thermocouples.
- Twelve band heaters positioned around the cylindrical vessel to control heat losses. These comprised six half-moon-shaped, 0.064-m bands uniformly distributed over the vessel's top half, and another six over its bottom half. Each of these heaters was operated by a separate controller.
- A pressurized and insulated fully-automated production system encompassing four production tanks, each with a capacity of 18 L.
- Perforated stainless steel tubes, each 0.025 m in diameter, for the horizontal injector and producer. These tubes were covered with a stainless-steel mesh to prevent sand production during the experiments.
- High-pressure water and solvent injection pumps rated at approximately 34000 kPa.
- Data acquisition system to monitor and record process parameters.
- A wet test meter to measure the amount of gases produced.
- An online gas chromatograph to analyze the composition of the produced gas.
- High-temperature fiber-wool insulation paired with Kevlar sheaths, tailored for the cylindrical vessel and the end flanges, to reduce heat losses.
- One steam generator with a power rating of 15 kW.

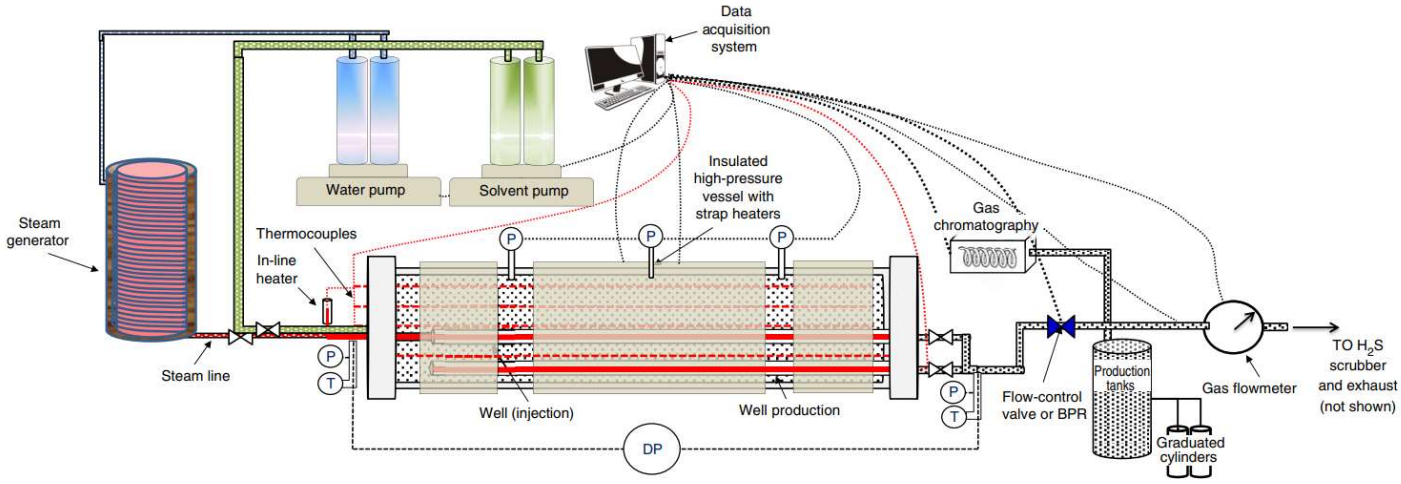

Fig. 2—A schematic diagram illustrating the experimental setup used for SAGD and DME-SAGD. In the schematic, BPR stands for backpressure regulator, DP for pressure transducer, P for pressure gauge, and T for temperature gauge. H_2S is hydrogen sulfide.

Figure 3 depicts the distribution of the 19 TCs and the locations of the horizontal injector and producer on a vertical cross-section. The injector was situated 0.12 m from the vessel's base, while the producer was at 0.04 m. These 19 TCs were spread across five evenly spaced vertical planes in the longitudinal direction (Figure 3b). The experimental setup also had three pressure gauges. Furthermore, a heat loss control system controlled the external band heaters, inline well heaters, and both the production and injection flanges.

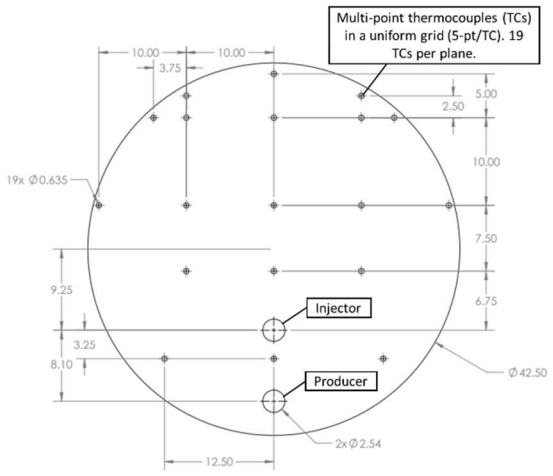

(a) Locations of horizontal wells and 19 thermocouples (TCs) on a vertical cross-section. Dimensions are in centimeters.

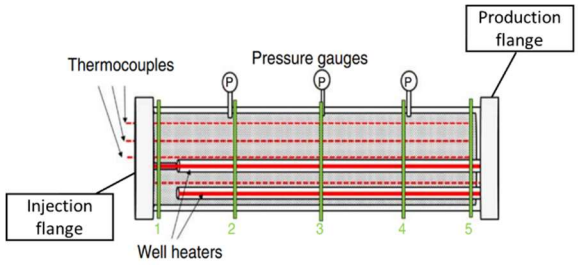

(b) A longitudinal cross-section of the 3-D cylindrical model. The five vertical cross-sections given by green lines are used in the analysis of experimental data in this paper. It also shows three pressure gauges and the injection and production flanges. The injection and production horizontal wells were surrounded by inline heaters.

Fig. 3—Locations of horizontal wells and 19 TCs in the cylindrical model for the SAGD and DME-SAGD experiments.

Bitumen Properties

The bitumen sample used in the SAGD and DME-SAGD experiments was taken from a thermal bitumen production site in Alberta, Canada. Its molecular weight was 540 g/mol. The original asphaltene content of the bitumen sample was 17 wt%. The mass density of the bitumen sample at 101.3 kPa was 1015 kg/m^3 at 15°C, 999 kg/m^3 at 40°C, and 974 kg/m^3 at 80°C. The viscosity of the bitumen sample at 101.3 kPa was 1.34×10^6 cp at 15°C, 30,957 cp at 40°C, and 808 cp at 80°C.

The bitumen was characterized using two pseudo-components, B1 (distillable) and B2 (non-distillable), with the Peng-Robinson (PR) EOS (1978). The vapor pressure properties (i.e., P_C, T_C, and ω) for these pseudo-components were estimated by following Kumar and Okuno's method (2016), as shown in **Table 1**. Furthermore, models for bitumen's density and viscosity were developed by matching the experimental data, as elaborated in the "Numerical Model" section.

	Mol %	MW, g/mol	T_c, °C	P_c, kPa	Acentric factor (ω)
B1	47.5	284.1	529.85	1500	0.1889
B2	52.5	771.8	933.15	767	0.4066

Table 1—Model parameters for bitumen's pseudo-components using the PR EOS. The binary interaction parameter between B1 and B2 is zero. The PR-EOS model was calibrated with the measured bitumen PVT data using Kumar and Okuno's (2016) method.

Experimental Procedure

Model Packing and Bitumen Saturation

The cylindrical vessel was dry-packed with 312 kg of synthetic unconsolidated dry sand. This packing process began after fitting one of the flanges, the injection and production wells, and thermocouple grids. The vessel was oriented vertically and filled with sand in batches, each compacted in place using a submersible cement vibrator. Following this, the vessel was sealed by installing the second flange. Leak tests were then conducted, after which the physical model was imbibed with deionized water at 23°C. The bulk volume of the vessel was 175.6 L, which was obtained after subtracting the volumes occupied by the horizontal wells and the thermocouple lines from the original model's total empty volume. For bitumen saturation, the physical model was heated to approximately 70˚C, and 1.2 PV of hot bitumen was injected from the bottom, displacing water from the top. **Table 2** summarizes the measured properties of the

sand pack for the SAGD and DME-SAGD experiments. Note that the sand pack permeability remained unchanged because the same sand batch was used throughout the experiments.

Model Preheating

After model packing, a preheating stage began using the inline heaters of the injector and producer wells. The heaters were gradually brought to 125°C and maintained for 24 hours. The top and bottom band heaters controlled the heat losses from the cylindrical vessel. This preheating procedure was the same for both experiments.

SAGD Experiment

The procedures for this SAGD experiment followed Sheng et al. (2021) but differed in operational parameters. The steam injection rate was 30 mL/min (CWE) at 3000 kPa for five days in this research, and 35-50 mL/min (CWE) at 3600 kPa over 7.2 days in Sheng et al. (2021). The steam injection stage started after the preheating. Steam of 100% quality was injected into the sand pack through the three injection ports along the injector. To ensure 100% vapor injection at the sand face, the set point temperature for the injector's inline heaters was gradually increased from 125°C to approximately 285°C over 10 hours. The SAGD experiment was divided into two periods. Period 1 referred to the first two days, whereas Period 2 included the subsequent duration of the experiment. The steam injection rate and pressure were maintained throughout both periods. However, this demarcation was crucial for history-matching SAGD experimental data, as explained in the "Simulation Model" subsection.

DME-SAGD Experiment

The DME-SAGD experiment included a 24-hour preheating period, followed by steam injection for another 24 hours at a rate of 30 mL/min (CWE) at 3000 kPa. Then, the DME-steam co-injection stage began and lasted for 54.81 hours, where 10 mol% DME and 90 mol% steam were co-injected. The co-injection involved DME at a rate of 11.3 mL/min (under pump conditions of 7°C and 3000 kPa) and steam at 27.6 mL/min (CWE). The preceding SAGD stage was essential in establishing effective hydraulic communication between the two wells. **Table 3** summarizes the various stages of the SAGD and DME-SAGD experiments, detailing their durations, operational conditions, and injection rates.

Controlling heat losses was necessary to facilitate the expansion of a steam chamber within the physical model while keeping an adequate liquid level above the producer at the operational injection rate. Early development of a steam chamber was desirable for bitumen production data to represent multiphase flow in the presence of a steam chamber. The heat loss control was effectively achieved through the vessel's band heaters, representing a no-heat-flux boundary (Sheng et al. 2022b). This heat-loss control system employed an automated control logic to regulate the heaters' set points. These set points were determined based on the average temperature readings from TCs placed at different locations—the model's top and bottom, as well as along the end flanges (injection and production sides). This configuration ensured that the temperatures maintained by the band heaters closely represented those within the physical model, thereby minimizing heat flux across its boundaries. Despite the effectiveness of the heat-loss control system, some heat losses inevitably occurred during the experiments, particularly at locations where temperatures were not directly measured, such as the side boundaries of the model. These unmonitored locations likely contributed to additional heat losses that were not compensated for by the heaters. Therefore, the calibration of the numerical model required the inclusion of heat losses to history-match the experimental data.

Depressurization/Cooling Stage

A depressurization/cooling stage followed the steam injection and DME-steam co-injection stages in the SAGD and DME-SAGD experiments, which spanned 23.5 hours and six hours, respectively. During this stage, all heaters—top, bottom, and inline well heaters—were turned off. Simultaneously, the steam injection pump, alongside the solvent injection pump in the case of the DME-SAGD experiment, was also shut down. This was coupled with turning off the injection and production valves on the end flanges. In the SAGD experiment, the nitrogen (N_2) purge started and lasted four hours to remove hydrogen sulfide (H_2S) gas in preparation for the post-run excavation of the sand pack. Subsequently, the physical model underwent a pressure depletion stage, decreasing from 3000 kPa to atmospheric pressure over 19.5 hours for SAGD and six hours for DME-SAGD. Notably, the N_2 purging stage was omitted in the DME-SAGD experiment because no H_2S gas was produced. H_2S production is indicative of aquathermolysis, which becomes greater by increasing the reaction temperature and the exposure time of asphaltene to steam (Ovalles, 2019). That is, aquathermolysis seems to have slowed down for the DME-SAGD experiment because of the lower T_{edge} and the shorter time to achieve ultimate bitumen recovery in comparison to the SAGD experiment.

Handling of Produced Fluids

In each experiment, the produced liquid was collected by switching between two production tanks every two to three hours, facilitating frequent analysis of the produced fluid properties. Once the production tank became full, it was drained from the bottom line into graduated cylinders. The gas accumulated in the production tank underwent compositional analysis using gas chromatography, followed by volume measurement with a wet test meter. The procedure was identical to that used for dry gas produced from the physical model.

The composition of the produced liquids varied between experiments: the SAGD tanks contained water and bitumen, whereas the DME-SAGD tanks held DME, water, and bitumen. In both cases, water was separated from bitumen using toluene, and dissolved bitumen was also separated from water. **Table 4** provides a breakdown of the components within the three phases in the production

tanks for the DME-SAGD experiment. The W phase was designated as 100% water because DME was assumed to have negligible solubility in the W phase at standard conditions. Separating DME from bitumen presented technical challenges, as in the experiments by Amer et al. (2024b) and Pratama and Babadagli (2021). Therefore, the estimations of produced volumes (DME and bitumen) were based on the L phase mass density data and the ideal-mixing assumption. The ideal-mixing assumption was reasonable at standard conditions as the simulated bitumen and DME production histories matched the estimated data, as will be shown later.

Post-Run: Sand Pack Excavation

Following the depressurization/cooling stage, the physical model was cooled down to room temperature. The sand pack was excavated from the injection and production ends by dividing the sand pack equally into eight segments along the matrix. From each segment, three-to-four sand samples were taken where Dean-Stark analysis was performed to analyze their contents of sand, water, oil, and asphaltene weight%.

Case\Property	Bitumen volume at standard conditions, L	Porosity, %	Initial water saturation, %	Bitumen saturation, %	Permeability, D
SAGD	54.2	33.6	8.2	91.8	5.0
10 mol% DME-SAGD	55.4	33.2	4.9	95.1	5.0

Table 2—Measured properties for the sand pack used in the SAGD and DME-SAGD experiments, including bitumen volume, porosity, initial water saturation, bitumen saturation, and permeability.

(a) SAGD (the control experiment)

	Duration, hour	Operation pressure, kPa	Injection well temperature, °C	Injection rate, mL/min	Producer well temperature, °C
Preheat	24	3000	125		125
Steam injection	120	3000	235	Steam: 30	220
Total	144				

(b) DME-SAGD

	Duration, hour	Operation pressure, kPa	Injection well temperature, °C	Injection rate, mL/min	Producer well temperature, °C
Preheat	24	3000	125		125
Steam injection	22.65	3000	235	Steam: 30	220
DME-steam injection	54.81	3000	230	Steam: 27.6 DME: 11.3	212
Total	101.46				

Table 3—Operation conditions for (a) SAGD as the control experiment and (b) DME-SAGD, including stage duration, pressure, temperatures, and injection rates.

Phase	Components
Vapor (V)	DME and water
Oleic (L)	DME, bitumen, and water
Aqueous (W)	Water and bitumen

Table 4—Phase constituents (by components) in production tanks for the DME-SAGD experiment.

Experimental Results and Discussion

This section presents results for the SAGD and DME-SAGD experiments and their analysis. Most of the subsequent figures have labeled several stages of the experiment as listed in Table 3: preheat, steam injection (SAGD), and DME-SAGD.

Figure 4 shows the bitumen production histories for the SAGD and DME-SAGD experiments. The peak rate was 43.8 mL/min for the DME-SAGD experiment, which was more than twice greater than the two peak rates observed in the SAGD experiment. In the SAGD experiment, the first peak at 20.9 mL/min coincided with the onset of steam injection (marking the start of Period 1), and the second peak at 18.8 mL/min was observed when the steam chamber expanded vertically and reached the physical model's ceiling (the beginning of Period 2). The steam chamber location in the SAGD experiment can be interpreted reliably by using TC temperature readings because of the absence of volatile components in the system. The occurrence of the second peak production rate was attributed to the transition from countercurrent to concurrent as the dominant flow regime, which was also observed in the SAGD experiment by

Sheng et al. (2021). Following these peaks, the bitumen production rate for both experiments declined sharply, dropping below 2 mL/min after 80 hours.

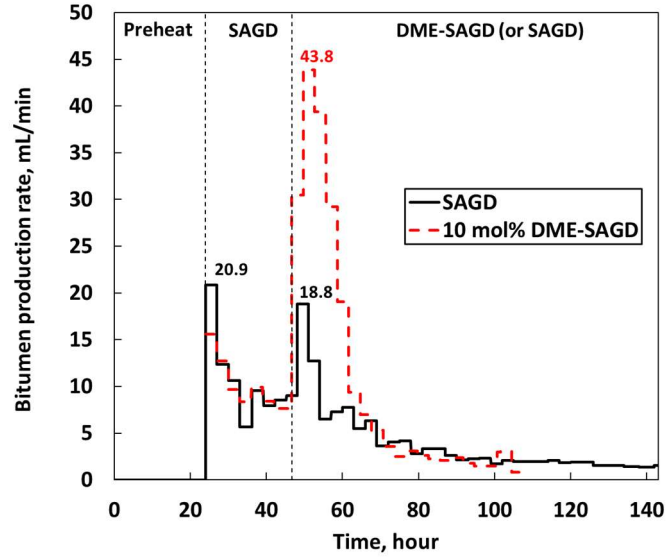

Fig. 4—Bitumen production rate histories for the SAGD and DME-SAGD experiments. The peak rate for the DME-SAGD experiment was 43.8 mL/min, which was more than twice greater than the two peak rates observed in the SAGD experiment.

Figure 5 compares bitumen cumulative recovery factors (RF) for the SAGD and DME-SAGD experiments. Bitumen RF was calculated by dividing the volume of produced bitumen by the initial bitumen volume at standard conditions (Table 2). The DME-SAGD experiment achieved an ultimate RF of 92.7%, markedly higher than the 68.6% RF of SAGD. Notably, the first 15 hours of the DME-steam co-injection yielded an incremental bitumen recovery of 53%. Note again that bitumen production estimates in the DME-SAGD experiment were derived from the measured L phase production data, as previously detailed. These estimates were compared against the SAGD results (Figure 5), and their accuracy was corroborated by the calibrated numerical model.

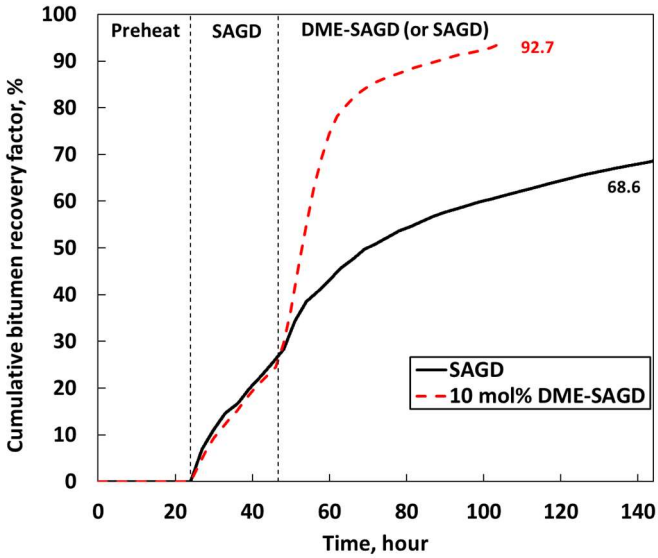

Fig. 5—Bitumen cumulative recovery factors (RF) for the SAGD and DME-SAGD experiments. The DME-SAGD experiment resulted in a greater ultimate bitumen RF of 92.7% in comparison to the SAGD experiment (68.6%).

The material balance calculations for both experiments are summarized in **Tables 5 and 6**. The material balance error percentage is defined as follows: Material balance error percentage for component i $(MBE\%)_i$ = [(cumulative volume injected)$_i$ – (cumulative volume produced)$_i$] / (cumulative volume injected)$_i$. In the SAGD experiment, 7.4% of the injected water was retained within the physical model and was not recoverable, even after applying N_2 purging and pressure depletion stages. Conversely, an additional 1.1% of water was produced in the DME-SAGD experiment, likely because the DME solubility in the W phase was assumed to be negligible under standard conditions. Furthermore, there was a loss of 13.2% of the injected DME volume, most likely because of retention within

the physical model and losses during fluid transfer. However, the calibrated numerical model suggested a higher DME recovery factor of 96.3% in comparison to the experimental estimate of 86.8%.

	Total water injected, standard L	Total water produced, standard L
	216	200
Difference	+16	+7.4%

Table 5— Material balance calculations for the SAGD experiment at standard conditions.

	Total water injected, standard L	Total water produced, standard L	Total DME injected, standard L	Total DME produced, standard L
	131.4	132.8	13149	11419
Difference	–1.4	–1.1%	+1730	+13.2%

Table 6— Material balance calculations for the DME-SAGD experiment at standard conditions.

Figure 6 shows the experimental cumulative steam-oil ratio (cSOR) plotted against the cumulative bitumen RF for the SAGD and DME-SAGD experiments. cSOR was calculated as the cumulative volume of steam injected (CWE) divided by the cumulative volume of bitumen produced. Note that the cSOR obtained from laboratory-scale experiments is expected to differ from those observed at a field scale qualitatively and quantitatively; the no-heat-flux boundary condition was imposed by the outer band heaters of the physical model in this experiment, as detailed earlier. The DME-SAGD experiment demonstrated a significant reduction in the ultimate cSOR by over 50% in comparison to the SAGD experiment in this research.

The reduction in cSOR for the DME-SAGD experiment can be attributed to a couple of key factors. First, the co-injection of solvent (DME) leads to a lowered condensation temperature (Keshavarz et al. 2015; Sheng et al. 2017), which effectively reduces the heat losses when compared with SAGD. Second, the co-injection of DME accelerates bitumen production and shortens the duration until the ultimate recovery is achieved (Table 3), thereby reducing the exposure time of the high-temperature vapor chamber to boundaries.

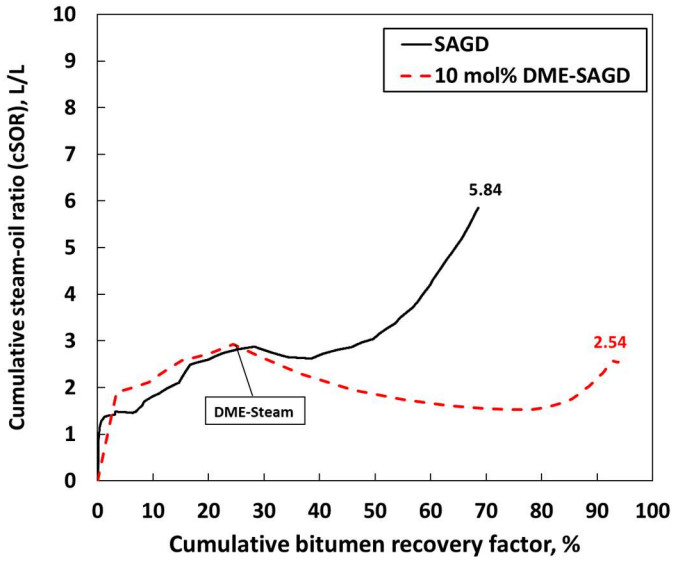

Fig. 6—Experimental cumulative steam-oil ratio (cSOR) plotted against cumulative bitumen recovery factor for the SAGD and DME-SAGD experiments. The DME-SAGD reduced the ultimate cSOR by more than 50% in comparison to SAGD.

Figure 7 shows the temperature distributions (measured and simulated) and simulated gas saturation distributions for the SAGD experiment across planes 2, 3, and 4 at the end of (a) Period 1 (2 days) and (b) Period 2 (6 days). Data from the 19 TCs and well locations were used to spatially interpolate temperatures within the circular plane using the cubic spline method. The boundary of a steam chamber in the SAGD experiment could be delineated from the 233°C contour line, corresponding to the saturation temperature of water at the operational pressure of 3000 kPa. Additionally, four other contour isotherms ranging from 215°C to 225°C are given in the figure. The data revealed a more pronounced expansion of the steam chamber for planes closer to the injection flange (planes 1, 2, and 3) than those near the production flange (planes 4 and 5), indicating a higher degree of heat loss on the production side of the physical model. The simulated temperature and gas saturation distributions reasonably agree with the measured temperature data.

(a) Period 1 (2 days)				
	Plane 2	Plane 3	Plane 4	Scale
Temperature contours, °C	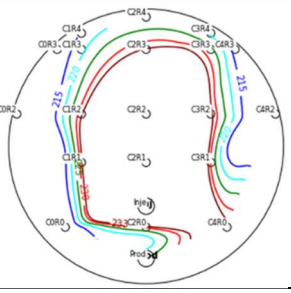	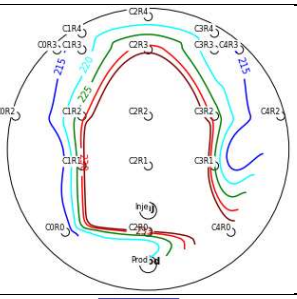	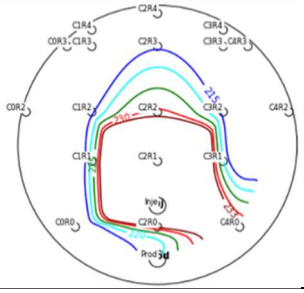	Isothermal contour lines from inside to outside: 233°C, 230°C, 225°C, 220°C, and 215°C
Simulated temperature distribution, °C	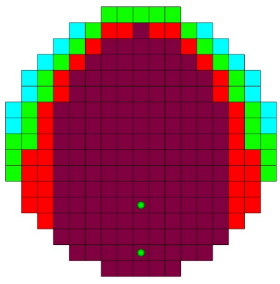	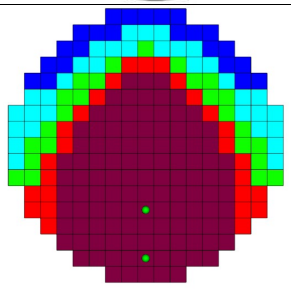	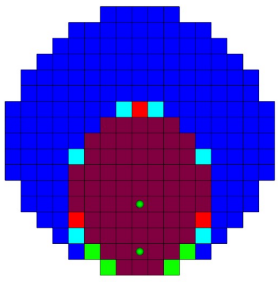	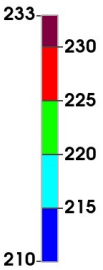
Simulated gas saturation (S_g) distribution	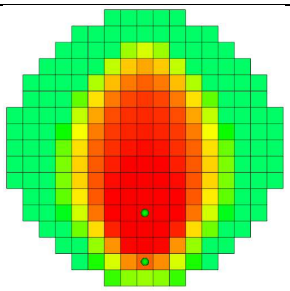	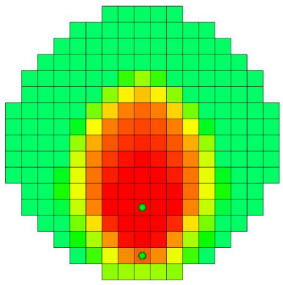	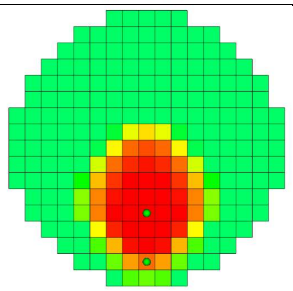	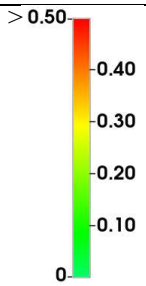
(b) Period 2 (6 days)				
	Plane 2	Plane 3	Plane 4	Scale
Temperature contours, °C	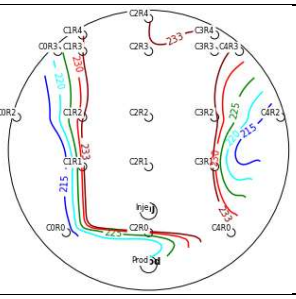	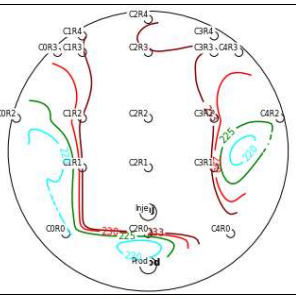	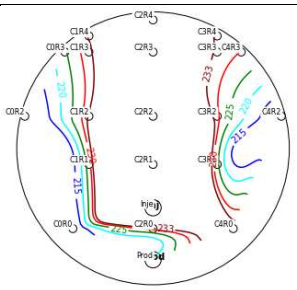	Isothermal contour lines from inside to outside: 233°C, 230°C, 225°C, 220°C, and 215°C
Simulated temperature distribution, °C	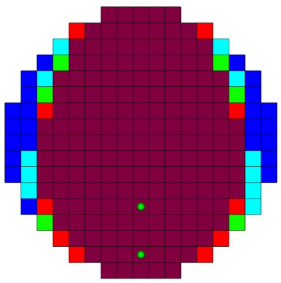	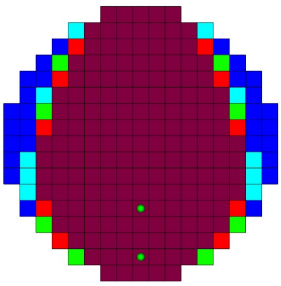	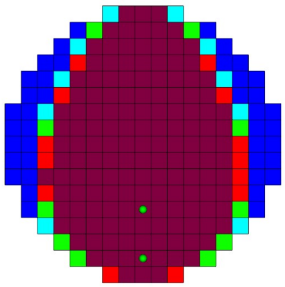	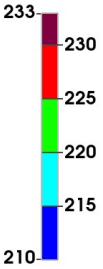
Simulated gas saturation (S_g) distribution	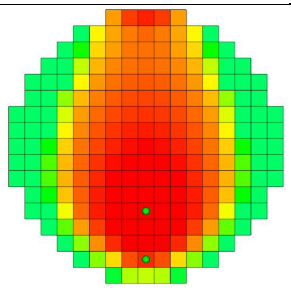	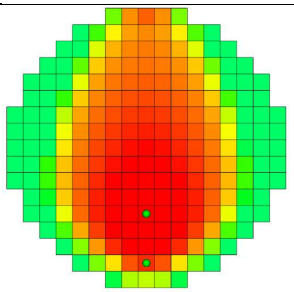	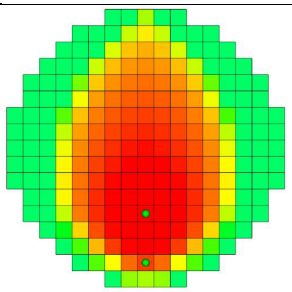	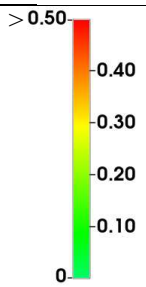

Fig. 7—Comparison between measured temperature distribution, simulated temperature distribution, and simulated gas saturation distribution for SAGD experiment at planes 2, 3, and 4 by the end of Period 1 (2 days) and Period 2 (6 days). Rows 3 and 8 show the measured temperature distributions at different vertical planes. Within each plane, 19 thermocouples (TCs) and 2 wells are indicated by white circles and are labeled in black.

Figure 8 shows the temperature distributions (measured and simulated) and simulated gas saturation distributions for the DME-SAGD experiment at planes 2, 3, and 4 at the end of (a) SAGD (2 days) and (b) DME-SAGD (4.2 days) stages. The simulated temperatures were slightly higher at the left and right boundaries of the model than the measured temperatures, but a good match was obtained along the vertical direction. Unlike the SAGD experiment, the temperatures near the edge of the DME-SAGD steam chamber were sensitive to the local fluid compositions; therefore, it was not possible to indicate the expansion of a steam chamber solely based on the temperature profiles. However, these temperature contours were instrumental to successful history-matching, as will be shown in the next section.

Figure 9 compares the produced bitumen properties: (a) viscosity, (b) asphaltene weight%, and (c) mass density from the SAGD and DME-SAGD experiments. The SAGD experiment demonstrated in-situ bitumen upgrading with the mass density reducing from the original 1015 kg/m^3 to 1007 kg/m^3, and the asphaltene weight% decreasing from the original 17 wt% to an average of 11 wt%. The DME-SAGD experiment at 3,000 kPa showed a similar level of in-situ upgrading to SAGD. In contrast, Sheng et al. (2022b) observed less in-situ upgrading in their 2.8 mol% condensate-SAGD experiment in comparison to SAGD at 3,500 kPa, using the same large-scale physical model (Figure 4). This disparity in the in-situ upgrading levels can be attributed to the differences in T_{edge} between SA-SAGD and SAGD in these scenarios. The T_{edge} difference between DME-SAGD and SAGD at 3,000 kPa is likely smaller than that between condensate-SAGD and SAGD at 3,500 kPa, potentially due to the DME's slight polarity.

Figure 10 shows photos of the excavated sand pack following the SAGD and DME-SAGD experiments. Several samples taken from the sand pack were analyzed for oil, water, and solid (OWS) content and asphaltenes weight%. In the SAGD experiment, the matrix ends showed lower oil recovery, with an average remaining oil saturation (S_{or}) of 41%. The average S_{or} was approximately 15% within the grey-highlighted steam chamber area, leading to an overall area-weighted average S_{or} of 26.2%, which was consistent with the bitumen recovery data. The average asphaltene weight percentage was 19.5% for all the samples taken from the excavated sand pack.

For the DME-SAGD experiment, the matrix ends also exhibited lower bitumen recovery, with an average S_{or} of 21%. The average S_{or} was 13% directly above the production well, which was roughly 6% smaller than the ultimate bitumen RF. The average asphaltene weight percentage was slightly greater at 22% for all the samples taken from the excavated sand pack. Furthermore, no asphaltene precipitation was observed near the wellbores. **Figure 10b** shows swirl-like patterns throughout the matrix without a distinct vapor chamber in any vertical cross-section for DME-SAGD likely because a rapid pressure reduction in the wind-down stage could have resulted in local boiling of DME from the L and/or W phases. Appendix B presents Dean-Stark analysis results for the samples taken from the excavated sand pack for SAGD and 10 mol% DME-SAGD.

(a) SAGD stage (2 days)				
	Plane 2	Plane 3	Plane 4	Scale
Temperature contours, °C	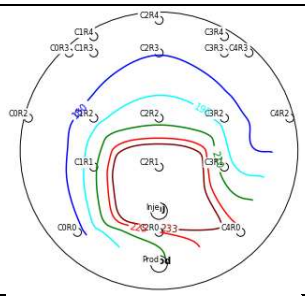	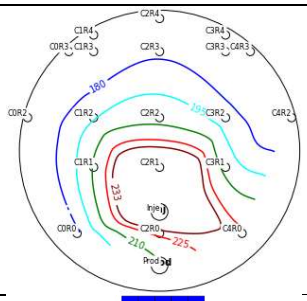	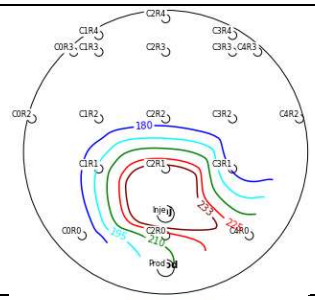	Isothermal contour lines from inside to outside: 233°C, 225°C, 210°C, 195°C, and 180°C
Simulated temperature distribution, °C	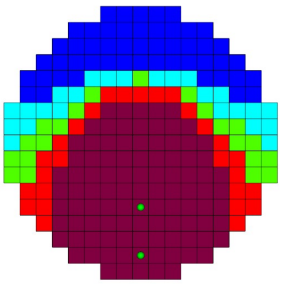	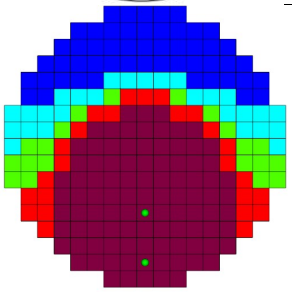	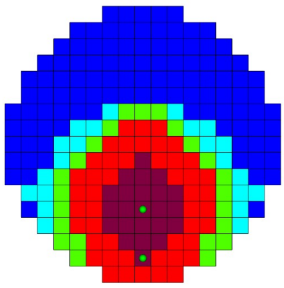	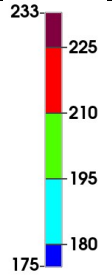
Simulated gas saturation (S_g) distribution	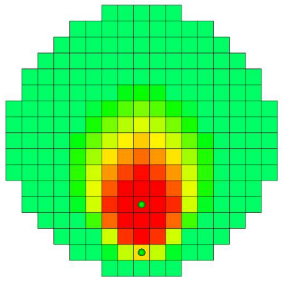	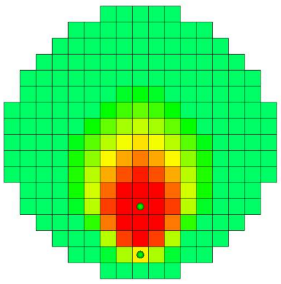	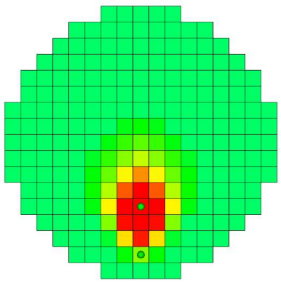	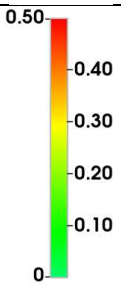
(b) DME-SAGD stage (4.2 days)				
	Plane 2	Plane 3	Plane 4	Scale
Temperature contours, °C	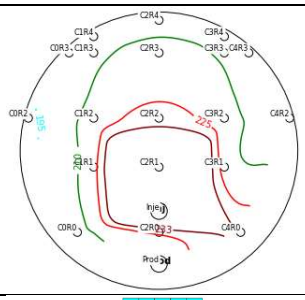	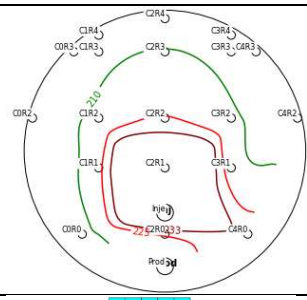	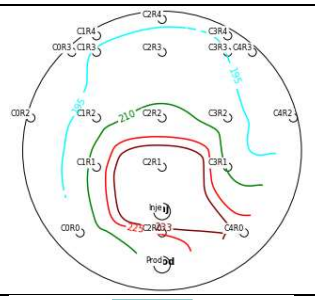	Isothermal contour lines from inside to outside: 240°C, 225°C, 210°C, 195°C, and 180°C
Simulated temperature distribution, °C	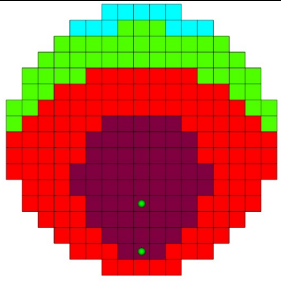	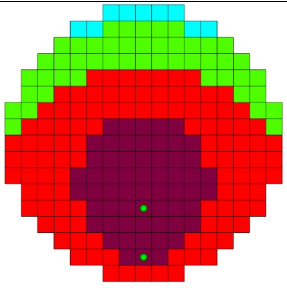	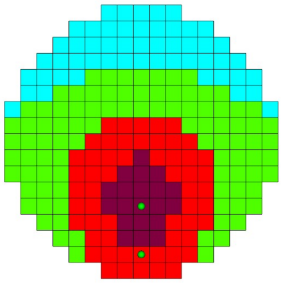	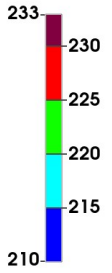

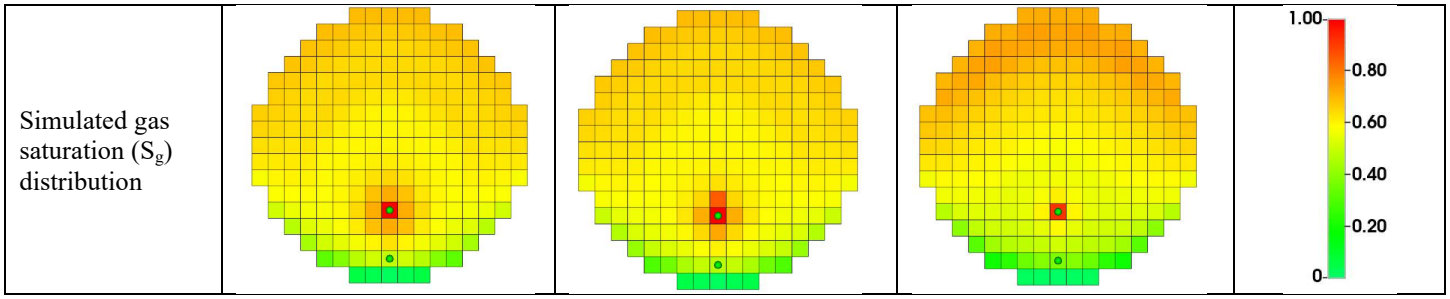

Fig. 8—Comparison between measured temperature distribution, simulated temperature distribution, and simulated gas saturation distribution for the 10 mol% DME-SAGD experiment at planes 2, 3, and 4 by the end of (a) SAGD (2 days) and (b) DME-SAGD (4.2 days) stages. Rows 3 and 8 show the measured temperature distributions at different vertical planes. Within each plane, 19 thermocouples (TCs) and 2 wells are indicated by white circles and are labeled in black.

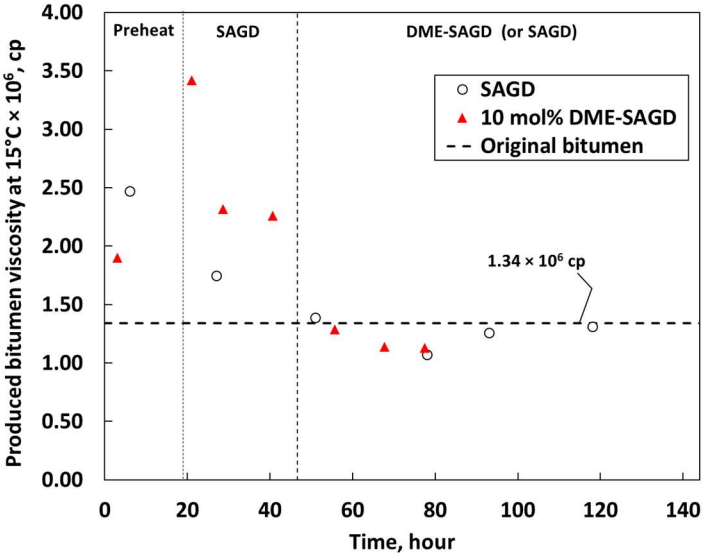

(a) Produced bitumen viscosity

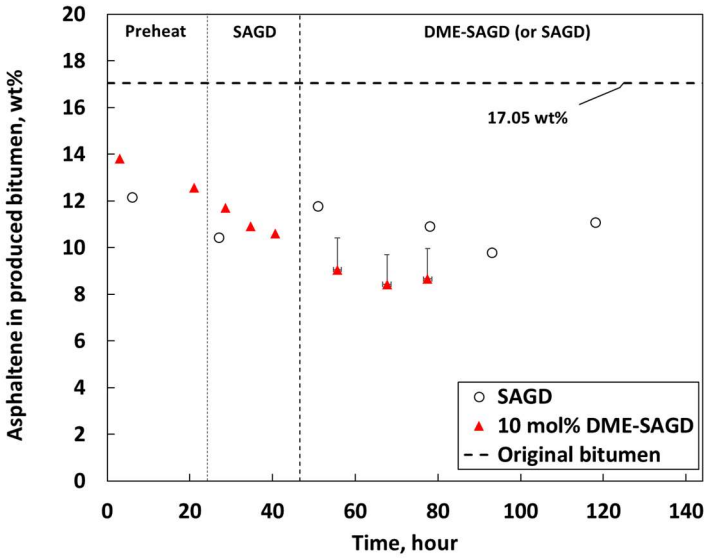

(b) Produced bitumen asphaltene weight%. The error bars represent the variation in asphaltene weight percentage during the DME-SAGD stage. The lower limit of the error bars corresponds to the asphaltene content assuming DME-free bitumen, and the upper limit represents the corrected asphaltene weight percentage, based on the maximum estimated DME solubility in bitumen of 15 weight%.

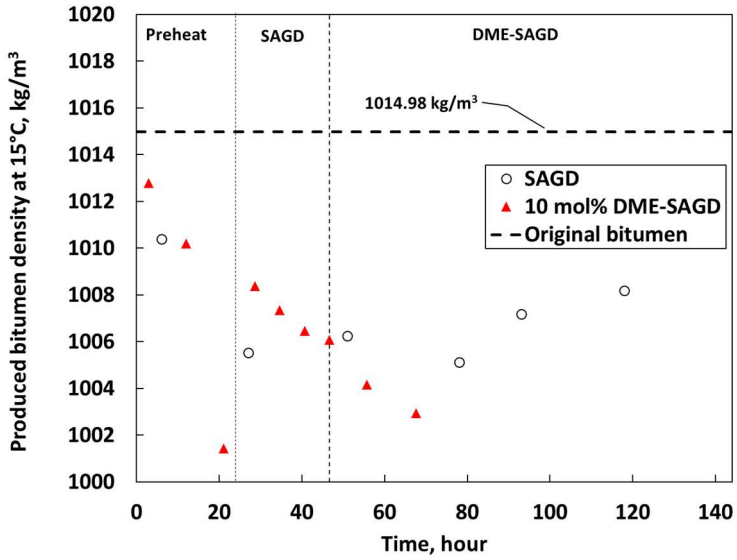

(c) Produced bitumen mass density

Fig. 9—Comparison of the produced bitumen quality in terms of (a) viscosity, (b) asphaltene weight%, and (c) mass density for the SAGD and 10 mol% DME-SAGD experiments. The dashed line refers to data of the original bitumen as a reference.

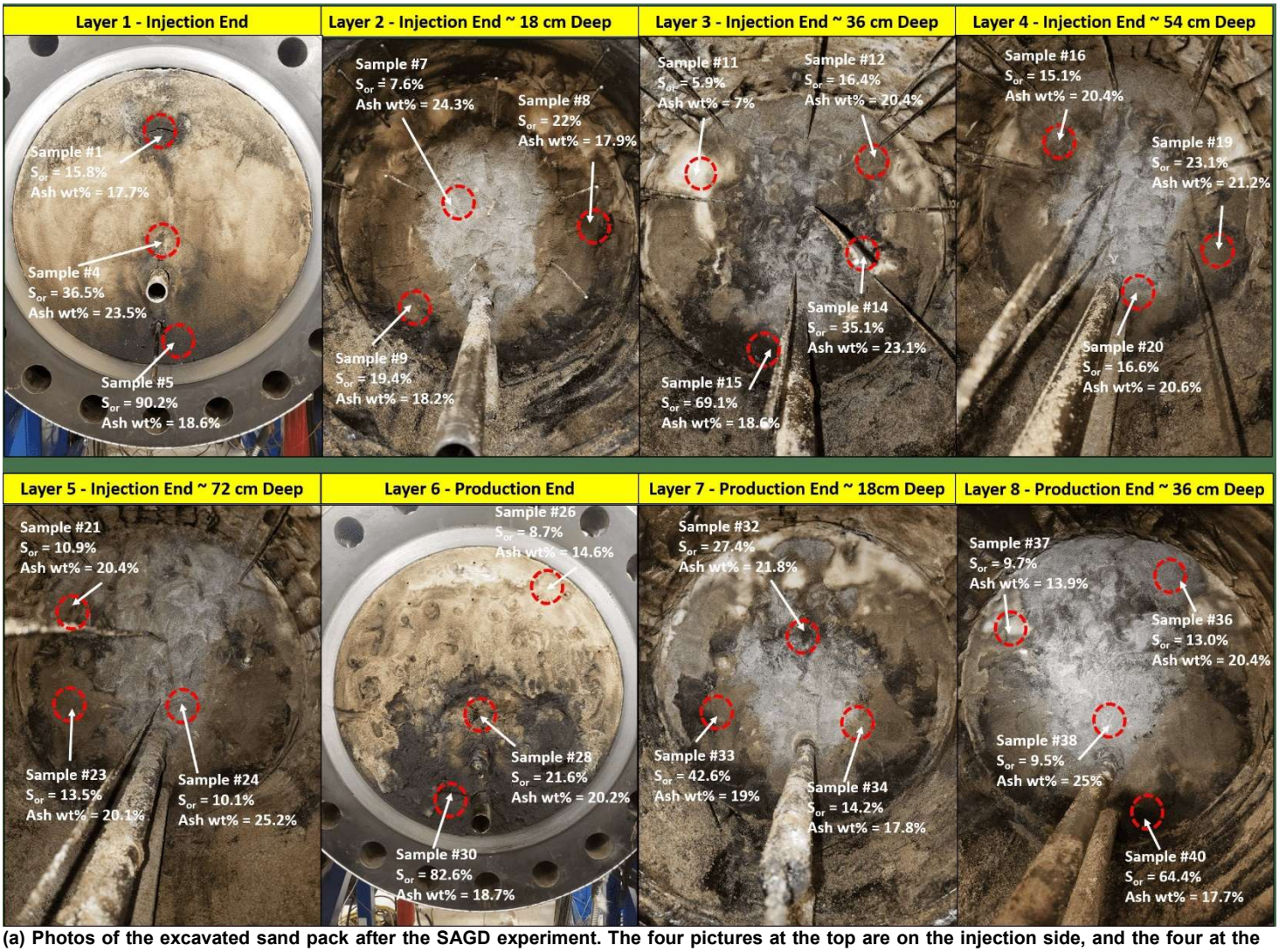

(a) Photos of the excavated sand pack after the SAGD experiment. The four pictures at the top are on the injection side, and the four at the bottom are on the production side.

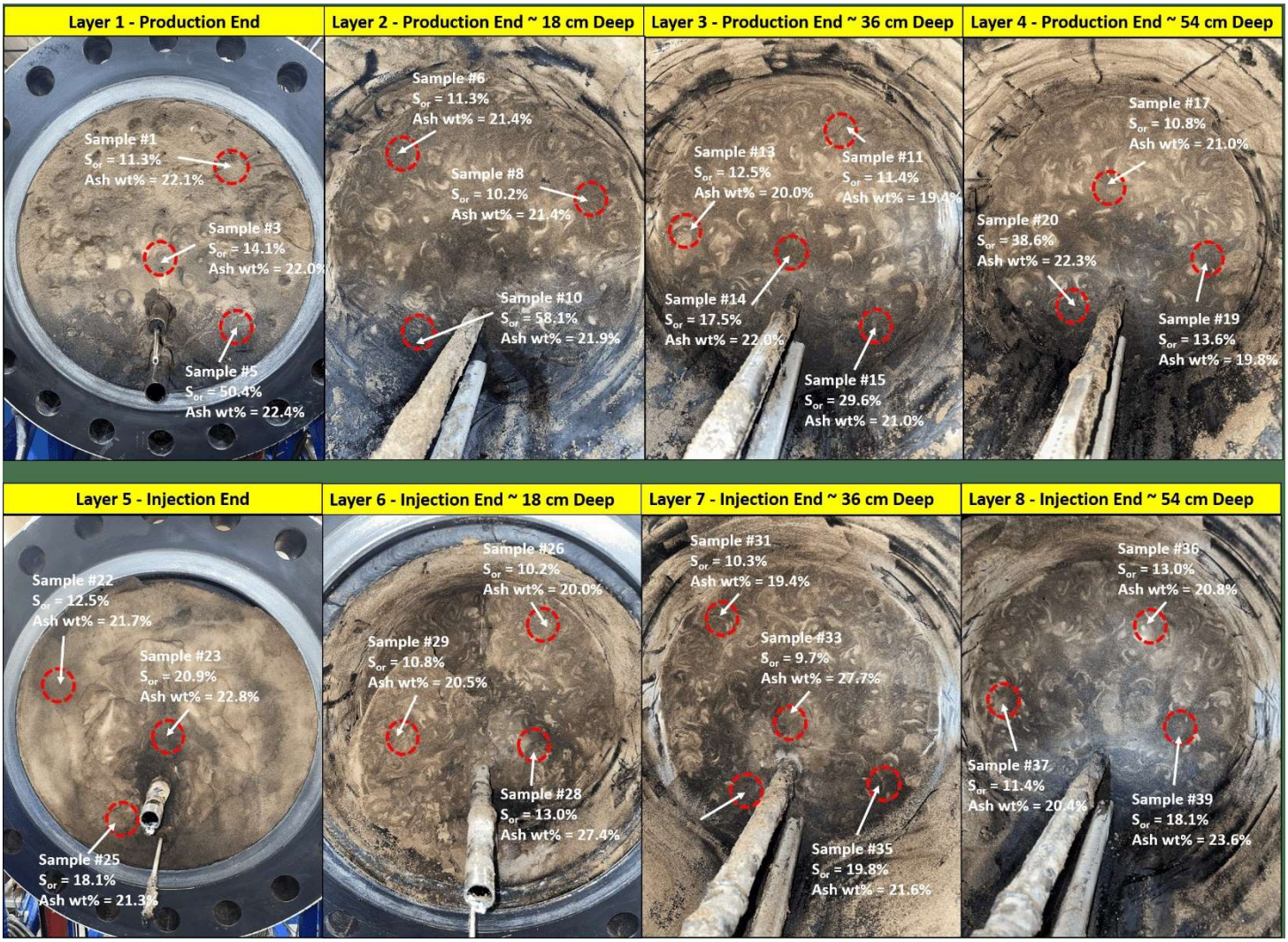

(b) Photos of the excavated sand pack for the DME-SAGD experiment. The four pictures at the top are on the production side, and the four at the bottom are on the injection side.

Fig. 10—Photos of the excavated sand pack after the (a) SAGD and (b) DME-SAGD experiments. Each dotted circle denotes locations where samples were taken for Dean-Stark analysis. Remaining oil saturation and asphaltene weight% in the remaining oil are also labeled in white beside each dotted circle.

Simulation Model and History Matching

Simulation Model

The thermal compositional simulator of Computer Modelling Group (2023), STARS, was used to perform compositional flow simulations, where phase behavior was modeled by K values. **Figure 11** gives an overview of the numerical model representing the dimensions of the experimental setup (Figure 3). The Cartesian coordinate model consisted of 17 × 29 × 17 grid blocks in the *I*, *J*, and *K* directions (a total of 8381 grid blocks) with a uniform grid block size of 2.5 × 4.9 × 2.5 cm^3. The model included two horizontal wells (an injector and a producer) along the *J* direction through the sand pack, replicating the continuous injection and production in the actual physical model. The model initial conditions were set directly using experimental data of fluid saturations for water and oil from each experiment. Temperature readings from the end flanges and inline well heaters, along with injection and production pressures, served as input data for the numerical simulation.

The fluid model consisted of four components: water, DME, and two bitumen pseudo-components, namely "distillable" B1 and "non-distillable" B2. Because DME partitions into the three phases for DME-SAGD simulations, two sets of K value tables (V-L and L-W) were generated by re-calibrating the PR EOS with the HV mixing rules based on Sheng et al. (2018). Specifically, van der Waals (vdW) mixing rules were applied for DME and the two bitumen pseudo-components (B1 and B2) by matching data of DME-bitumen mixtures from Haddadnia et al. (2018b). Similarly, vdW mixing rules between water and B1 and B2 were calibrated using Venkatramani and Okuno (2016). The binary interaction parameter was set to 0.0404 for DME/B1, 0.0638 for DME/B2, 0.2094 for water/B1, and 0.1694 for water/B2.

The L phase density was calculated using the ideal mixing of pure components, as implemented in STARS. The L phase viscosity was calculated using the modified Arrhenius model within STARS.

History-matching the SAGD experiment was conducted over two periods: the initial two days (Period 1) and the subsequent duration of the experiment (Period 2). For the DME-SAGD experiment, history-matching was similarly segmented into the initial SAGD stage (first 2 days) and the DME/steam stage (thereafter). Adjustments were made only to relative-permeability and heat-loss parameters during history-matching; other parameters, including capillary pressure, remained unchanged. Each period used a distinct set of relative-permeability and heat-loss parameters for history-matching, in which the SAGD stage of the DME-SAGD experiment had the same set of relative permeability as Period 1 of the SAGD experiment. **Appendix A** gives the modified parameters of heat loss and relative permeability after history matching. Note that the heat loss directions set in the simulation correspond to the sand pack's *I*- and *K*-directions (sideways and over- and underburdens), as well as through the flanges in the *J*- and *K*-directions (along the wellbore and over- and underburdens).

The Stone I model was used to calculate the three-phase relative permeability within STARS. **Figures 12a and 12b** illustrate the matched oil-water and gas-liquid relative permeability curves, respectively. Furthermore, **Figure 13** shows the capillary pressure curves used based on the calculation method of Sheng et al. (2021). **Table 7** summarizes the interfacial tensions (IFT) for water/oil (σ_{ow}) and oil/gas (σ_{og}) for the SAGD simulation and the DME-SAGD simulation. The differences in IFT values arise from the partitioning of the DME into the three phases, resulting in reduced IFTs for DME-SAGD (Amer et al. 2024b).

Thermal conductivities of the sand pack and the water, oil, and gas phases were set at 177120, 51840, 10368, and 2880 J/(m×day×°C), respectively, and were not modified during the history matching. The sand-pack compressibility remained constant at 2.42×10^{-5} kPa^{-1} throughout all simulations.

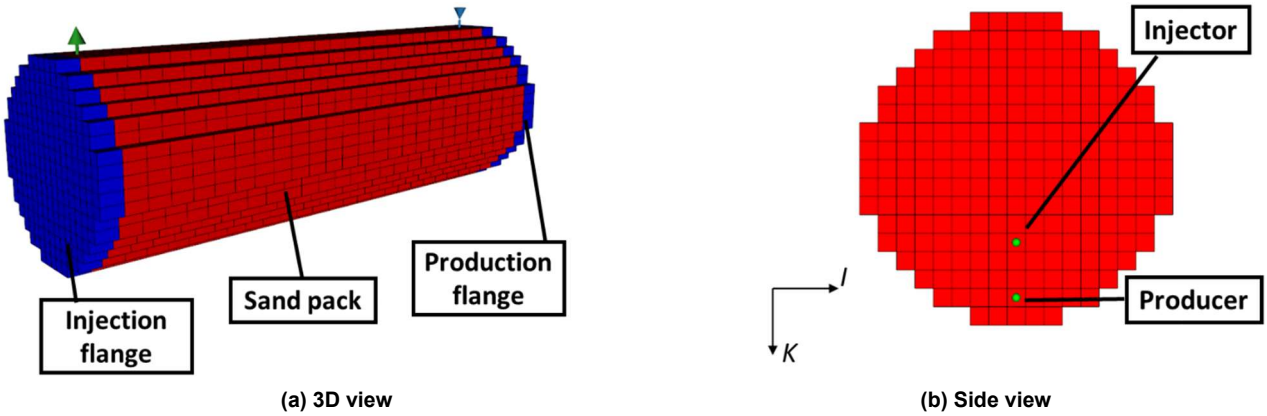

(a) 3D view (b) Side view

Fig. 11—A simulation model for the large-scale experimental setup. The numerical model consisted of three regions: injection and production flanges, and sand pack.

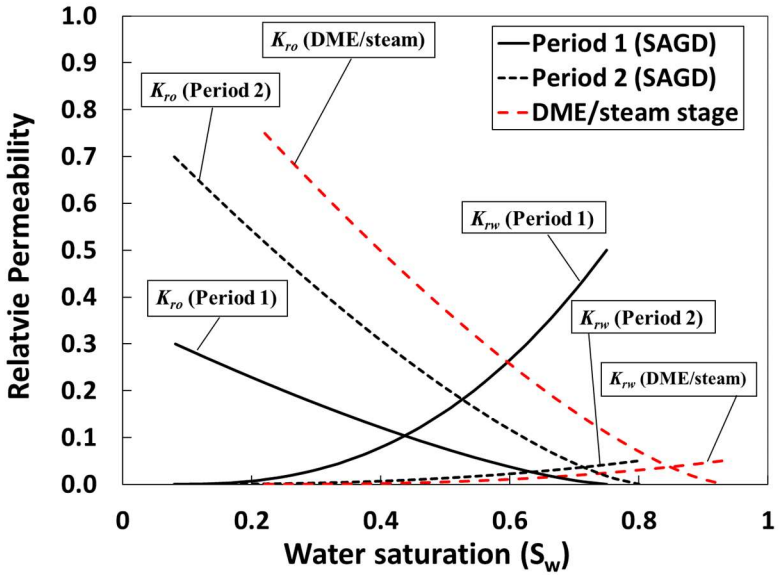

(a) Oil-water relative permeability models

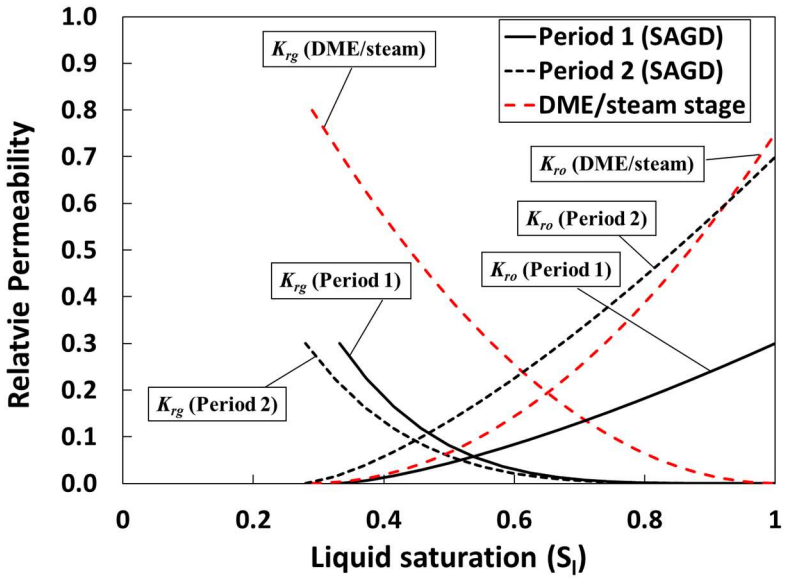

(b) Gas-liquid relative permeability models

Fig. 12— Relative permeability models used for history-matching SAGD and 10 mol% DME-SAGD experiments.

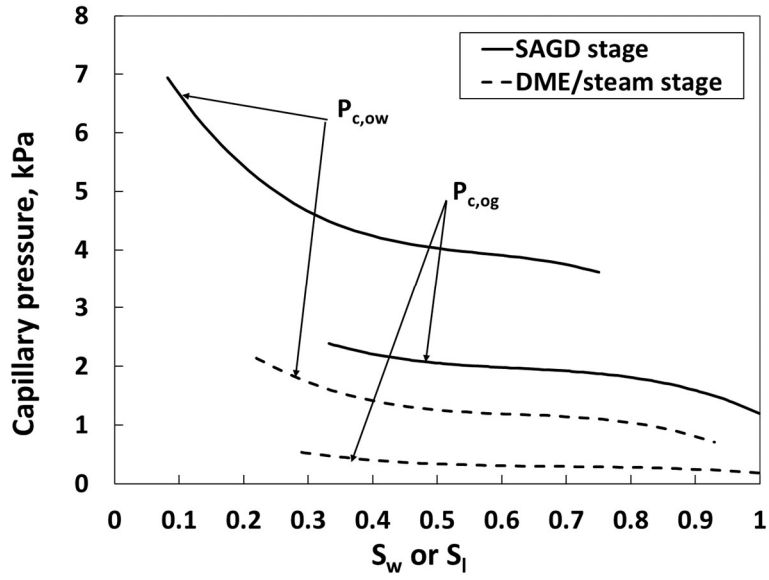

Fig. 13—Oil-water and gas-oil capillary pressure ($P_{c,ow}$ and $P_{c,og}$) curves used for SAGD and 10 mol% DME-SAGD simulations.

Stage	Water-oil IFT (σ_{ow}), dynes/cm	Oil-gas IFT (σ_{og}), dynes/cm	Reference
SAGD	30	15	Sheng et al. (2021)
DME/steam	9	2.25	Amer et al. (2024b)

Table 7— Water-oil and oil-gas interfacial tensions used for the SAGD and 10 mol% DME-SAGD history-matching simulations. IFTs were not changed during history matching for both experiments.

History Matching Procedure and Results

Sheng et al. (2021) noted some challenges in history-matching their SAGD experiment using the same experimental setup (Figure 3). The volume of a steam chamber in SAGD tends to be sensitive to the condensation of water because the SAGD fluid system has fewer condensable volatile components than SA-SAGD (a lower degree of freedom). Consequently, part of the sand pack in the SAGD experiment was swept by hot water, and the inclusion of capillary pressure data was important for matching temperature and

compositional material balance data. Note that this history-matching approach is specific to these laboratory-scale experiments, considering the physical model configuration and operational conditions used.

SA-SAGD, however, benefits from the existence of additional volatile components that sustain a steam chamber while releasing the latent heat near thermal fronts. Sheng et al. (2023) pointed out the importance of volatile species for maintaining a steam chamber and showed an efficient chamber expansion through tortuous hydraulic paths at lower temperatures than the steam temperature in their experimental study.

History-matching SAGD experimental data in this research followed the procedure outlined in Sheng et al. (2021). First, capillary pressure data (Figure 13) was included to model transitions in the flow regime from countercurrent to cocurrent as the steam chamber expanded and reached the ceiling of the model. Second, the simulation was divided into two periods (Period 1 and Period 2). Each simulation period required a distinct set of relative permeability (Figure 12) and heat loss parameters (Appendix A). Differences in relative permeability between cocurrent flow (Period 2) and countercurrent flow (Period 1) were explained in the literature (e.g., Bourbiaux and Kalaydjian 1990; Kalaydjian 1990; Bentsen and Manai 1993; Nasr et al. 2000).

History-matching the DME-SAGD experiment also required dividing the simulation into two periods: the SAGD and DME/steam stages. This division was essential because DME co-injection lowers IFTs as DME was partitioned into three phases (Pratama and Babadagli 2020; Lee et al. 2021; Zhao et al. 2023; Amer et al. 2024b). In addition, the flow regimes were different between the two periods, which required different sets of relative permeability for matching temperature and material balance data. Notably, DME-SAGD demonstrated a higher oil-water relative permeability than SAGD Periods 1 and 2; that is, DME-SAGD improved the oil mobility in the mixing zone, as shown in the next section. Note again that the SAGD stage of the DME-SAGD experiment was history-matched using the same relative permeability data as Period 1 of SAGD. **Figure 14** illustrates the history-matching procedure for the DME-SAGD experiment.

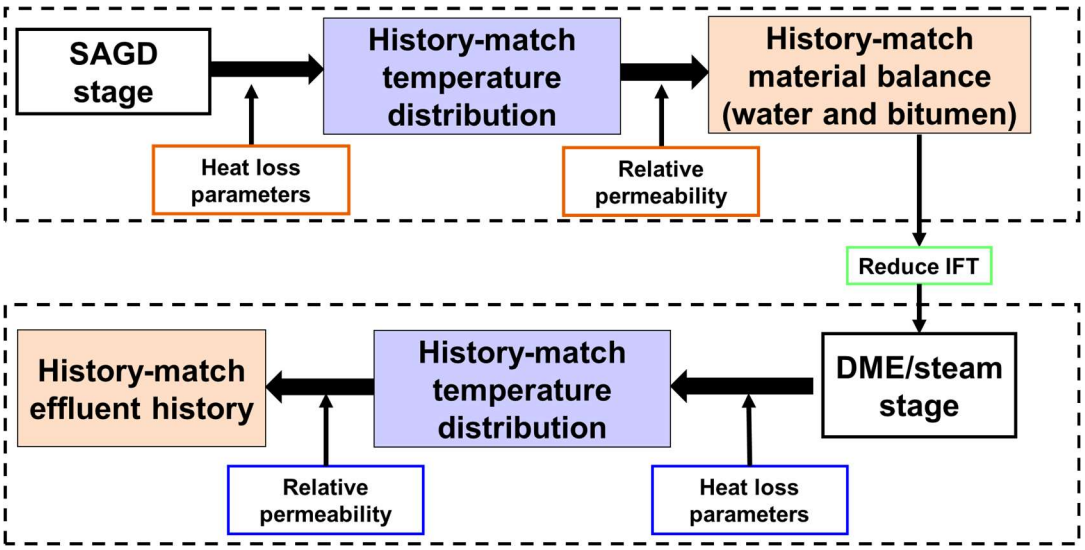

Fig. 14—Iterative procedure of history-matching the 10 mol% DME-SAGD experiment.

Figures 15 and 16 present compositional material balance data (measured and simulated) for the SAGD and DME-SAGD cases. For both experiments, the material balance for injection fluid (water for SAGD, and water and DME for 10 mol% DME-SAGD) was perfectly matched. However, the simulated DME production was higher than the estimation from the experimental data. Note again that DME was not completely separated from the other produced fluids for the DME-SAGD experiment. Therefore, the history-matching procedure relied on the effluent (water, DME, and bitumen) production data (Figure 16a). Despite these challenges, a satisfactory match was obtained for bitumen production history (Figure 16d). This outcome indicates that the amount of DME produced with bitumen in this research can be reasonably estimated under the assumption of no volume change on mixing at standard conditions.

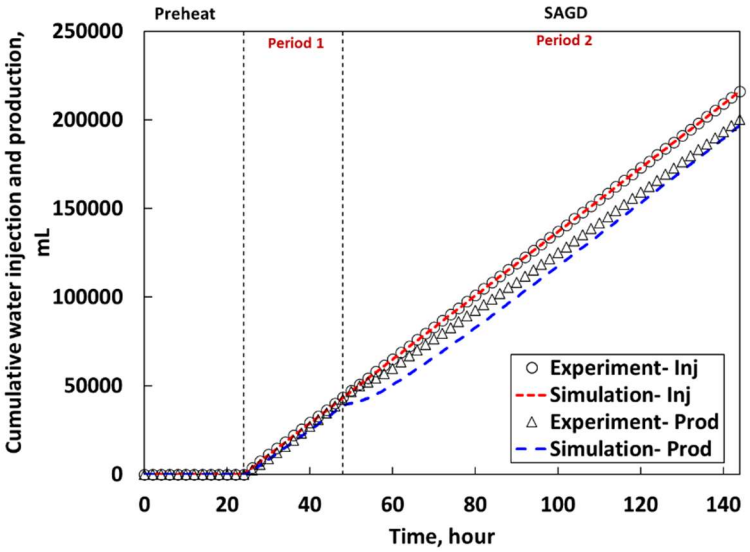

(a) Water material balance comparison

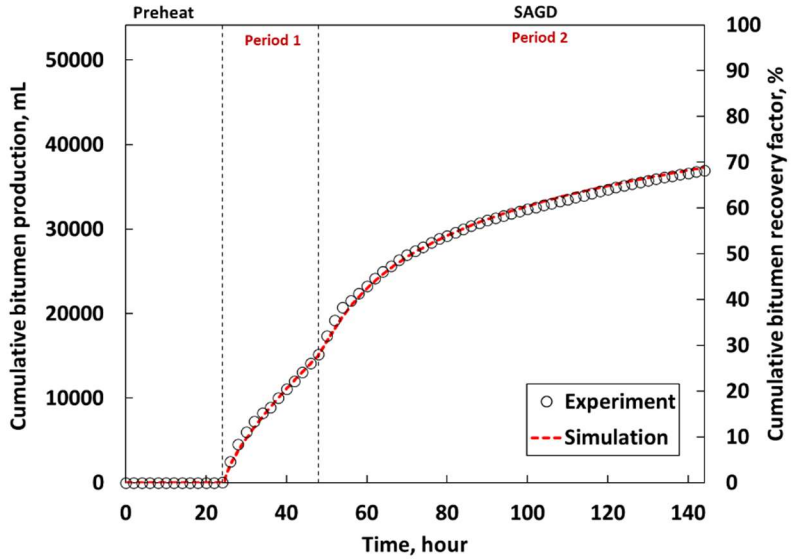

(b) Bitumen material balance comparison

Fig. 15—Comparison between simulated and experimental results for the SAGD experiment in terms of (a) water and (b) bitumen material balance.

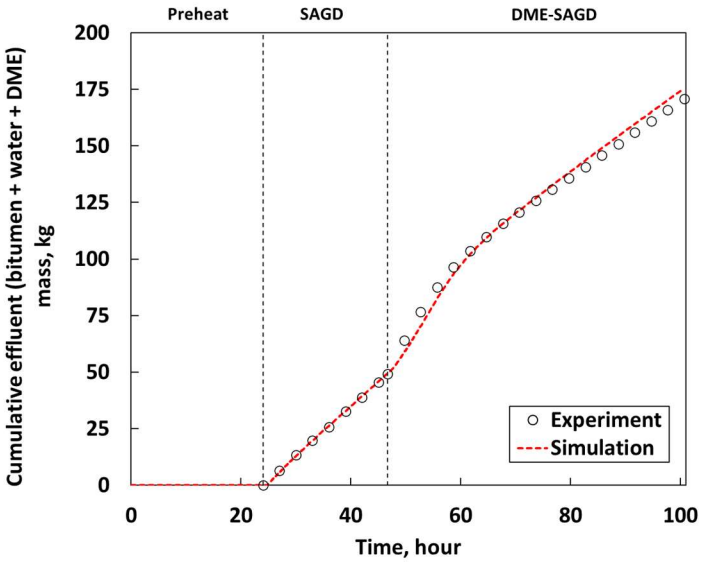

(a) Effluent (bitumen, water, and DME) production history comparison

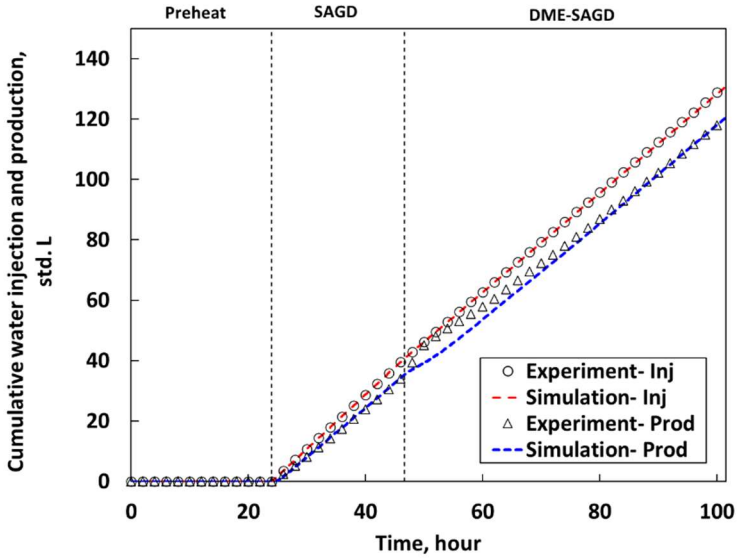

(b) Water material balance comparison

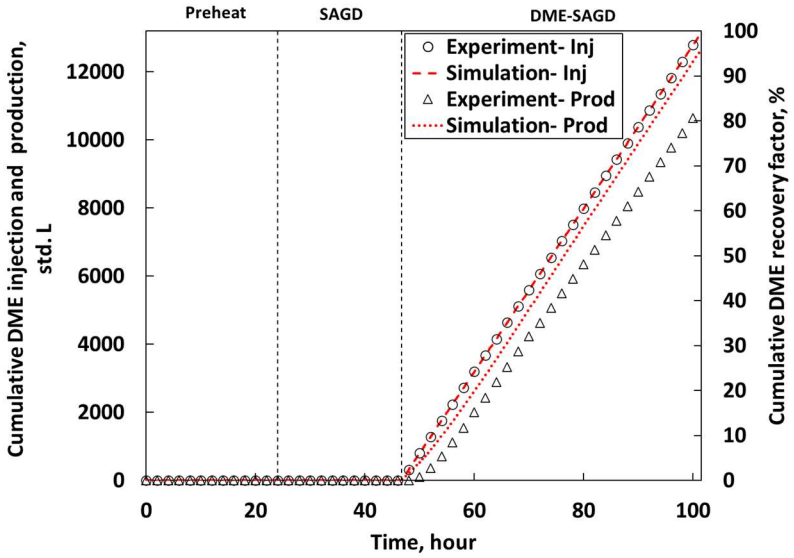

(c) DME material balance comparison. Experimental data underestimated DME production mostly because of DME mishandling during production tank switching. Simulated DME production shows 95% ultimate RF.

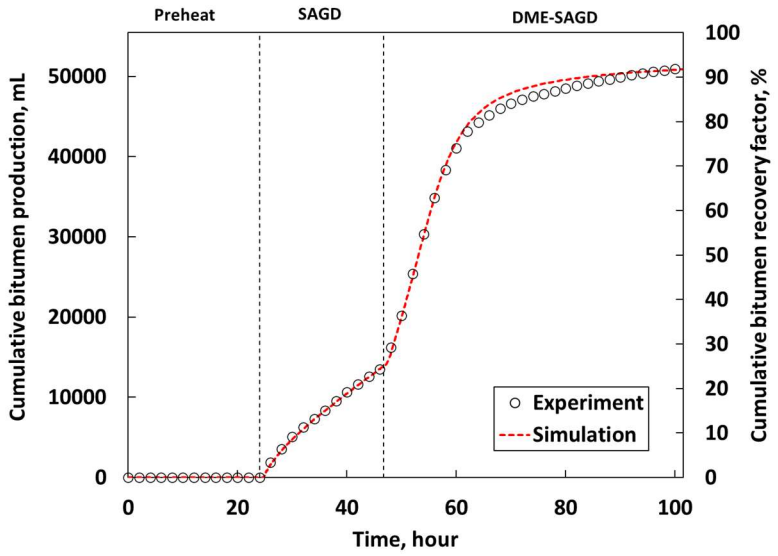

(d) Bitumen production history comparison

Fig. 16—Comparison between simulated and experimental results for the DME-SAGD experiment in terms of (a) effluent, (b) water, (c) DME, and (d) bitumen material balance.

Analysis Based on History Matching

The previous sections showed that the DME-SAGD experiment resulted in more effective bitumen gravity drainage than the SAGD experiment under the same experimental conditions. This section analyzes history-matching results for both cases in terms of energy requirement using local details based on 2-D maps from the calibrated numerical models.

One way to compare the energy efficiency of the experiments is to calculate the amount of energy used to produce a unit volume of bitumen for a system representing our large-scale physical model (Figure 3). We express the amount of energy used for bitumen production in terms of cumulative energy input (E_{in}) and cumulative net energy ($E_{in}-E_{out}$) divided by the cumulative bitumen production. E_{in} includes the energy input by the injection fluid and the heaters. E_{out} includes the energy output by the produced fluids. These calculations were based on the calibrated numerical models for both SAGD and DME-SAGD.

Figure 17a illustrates the energy used to produce a milliliter of bitumen (kJ/mL bitumen), plotted against the cumulative bitumen recovery factor (RF). The results indicate that 10 mol% DME-SAGD exhibited a smaller amount of energy consumption per unit volume of bitumen produced. The estimated energy consumption was 35.5 kJ/mL at the end of the SAGD experiment (RF = 68.6%), and it was significantly smaller at 14.7 kJ/mL bitumen at the end of the DME-SAGD experiment. On the net energy basis, the energy used for bitumen production remained greater for SAGD at 26.1 kJ/mL, while it was substantially less at 8.5 kJ/mL for DME-SAGD. Notably, DME-SAGD required only 2.4 days to recover the same volume of bitumen produced by six days of SAGD (Figure 6). The reduction in energy usage for DME-SAGD was mainly attributed to the accelerated bitumen production because of the enhanced mobility by dilution, and the lowered steam requirements for co-injection (Tables 5 and 6).

Figure 17b compares the carbon emission intensity, expressed in grams of CO_2 equivalent per milliliter of bitumen (gCO_{2eq}/mL bitumen), plotted against the cumulative bitumen RF for both experiments. The estimation of the gCO_{2eq} assumed 20 gCO_{2eq} per MJ of energy used for bitumen production (Gates and Larter 2014; Cai et al. 2015; Chai et al. 2023). The estimated carbon emission intensity was 0.71 gCO_{2eq}/mL at the end of the SAGD experiment, and it was significantly reduced to 0.20 gCO_{2eq}/mL bitumen for the 10 mol% DME-SAGD experiment. On a net energy basis, carbon emissions remained greater for SAGD at 0.52, while DME-SAGD demonstrated a notable decrease to 0.14 gCO_{2eq}/mL bitumen. It is important to note that the amount of CO_2 emissions due to DME synthesis was not included in the gCO_{2eq} estimations and was beyond the scope of this research. To the best of our knowledge, this is the first time the energy efficiency of DME-SAGD was experimentally studied and compared with SAGD.

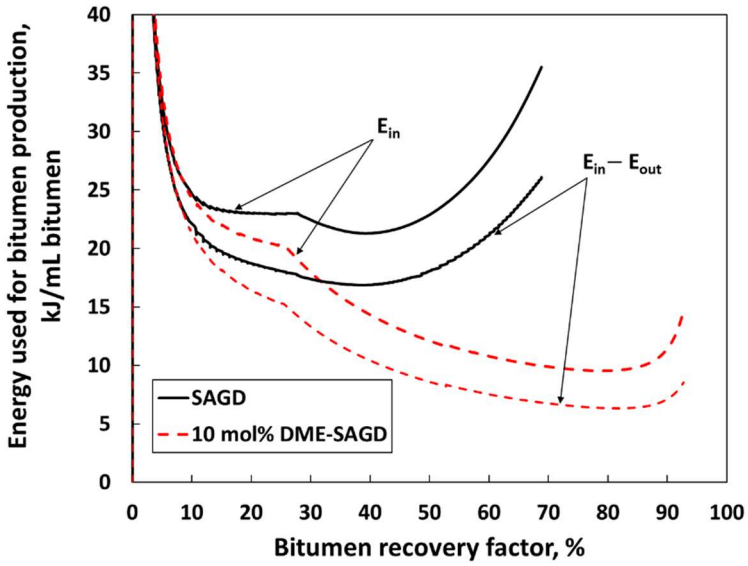

(a) Estimated energy used per unit volume of bitumen production

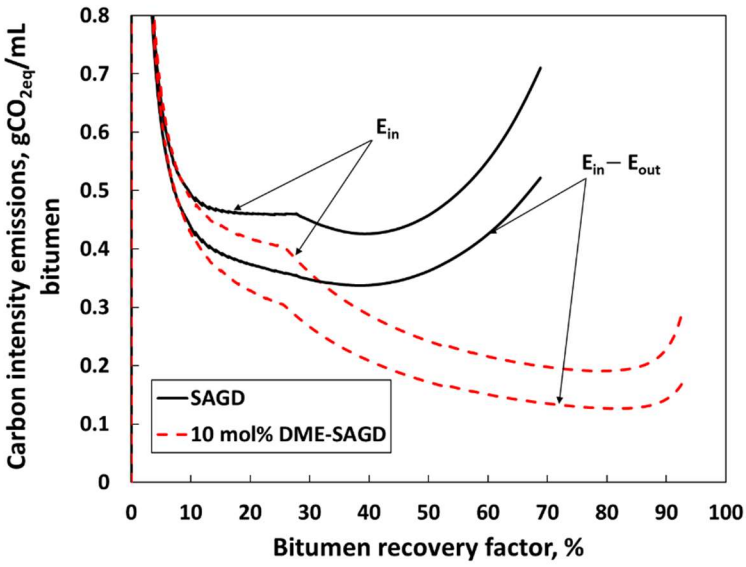

(b) Estimated carbon emission intensity per unit volume of bitumen produced

Fig. 17—Comparative analysis of SAGD and DME-SAGD in terms of (a) energy used per unit of bitumen produced and (b) carbon emission intensity, based on input energy (E_{in}) and net energy ($E_{in}-E_{out}$). The DME-SAGD experiment achieved equivalent bitumen recovery in 2.4 days—less than half the time required by SAGD—with over 50% energy savings and a minimum of 70% reduction in CO_{2eq} emissions.

Figure 18 displays 2D simulation maps based on the calibrated numerical models for the SAGD and DME-SAGD experiments. These maps were generated on the fourth vertical plane of the numerical model at time steps corresponding to a bitumen RF of 60% for both cases. Note that the analysis of these maps does not depend on the choice of the vertical plane because of the sand-pack homogeneity and the uniform distribution of injection and production ports along the wells.

Figure 18a shows the gas saturation maps for both cases where DME co-injection led to a more expanded steam chamber. SAGD's steam chamber was smaller because the fluid system exhibited narrow-boiling behavior with fewer volatile components than DME-SAGD (Zhu and Okuno, 2014). **Figure 18b** shows the temperature distributions for both cases, where the DME-SAGD experiment resulted in a lower T_{edge} compared to SAGD, thereby lowering the heat losses across the boundaries, as reflected in the energy requirements and carbon emissions for bitumen production (Figure 17). **Figures 18c and 18d** present the DME mole fraction in the L and W phases, respectively. DME-SAGD lowered the L-W IFT in comparison to SAGD, and also reduced the gravity segregation between the two phases (Sheng et al. 2018; Amer et al. 2024b).

Figure 18e shows the grid-scale Bond number (N_b), a dimensionless number calculated as the ratio of gravitational to interfacial forces based on the following equation:

$$N_b = \frac{(\rho_o - \rho_g) g r^2}{\sigma_{og}} \times 10^{-3},$$

where ρ_g is the V phase mass density, ρ_o is the L phase mass density, σ_{og} is the L-V interfacial tension, g is the gravitational constant, and r represents the average pore size of 100 μm. Notably, DME-SAGD gave a greater Bond number than SAGD, facilitating bitumen drainage by gravity (Stewart and Shaw, 2018). **Figure 18f** reveals that DME-SAGD led to a more uniform and smaller W phase distribution compared to SAGD because DME's mutual solubility yielded a reduced level of gravity segregation between the W and L phases. This uniform distribution of the L and W phases resulted in an overall increase in the L phase mobility (**Figure 18g**).

	SAGD	10 mol% DME-SAGD	Color legend
(a) Gas saturation	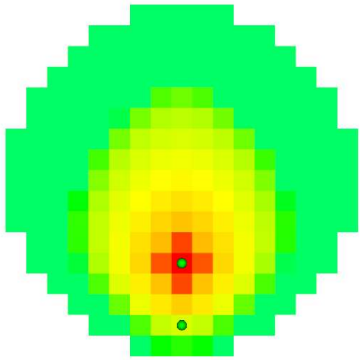	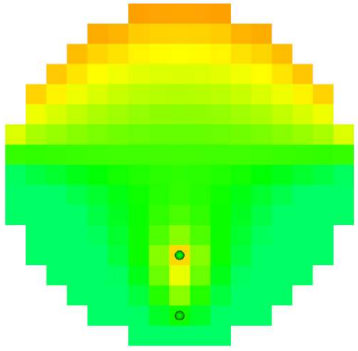	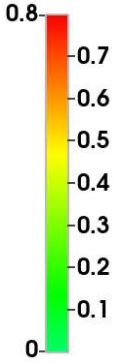
(b) Temperature, °C	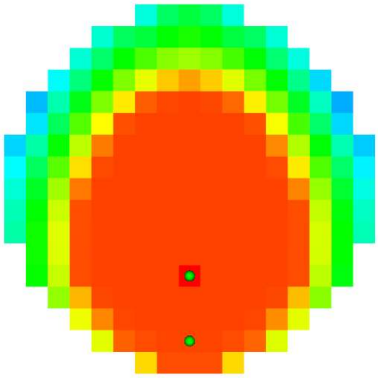	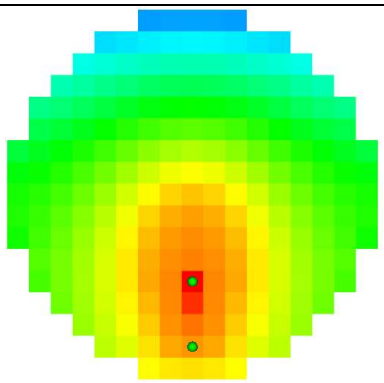	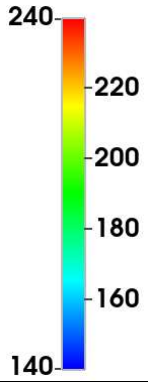
(c) DME mole fraction in L phase	N/A	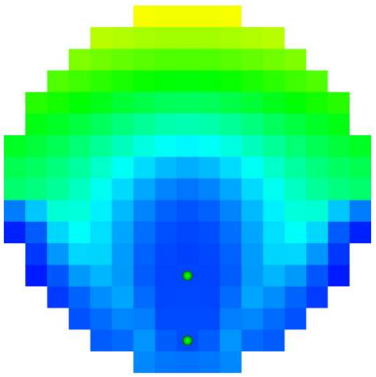	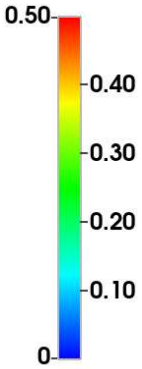
(d) DME mole fraction in W phase	N/A	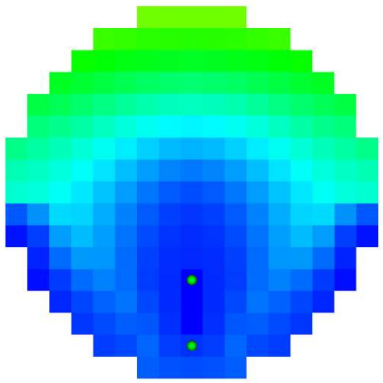	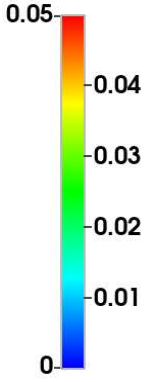

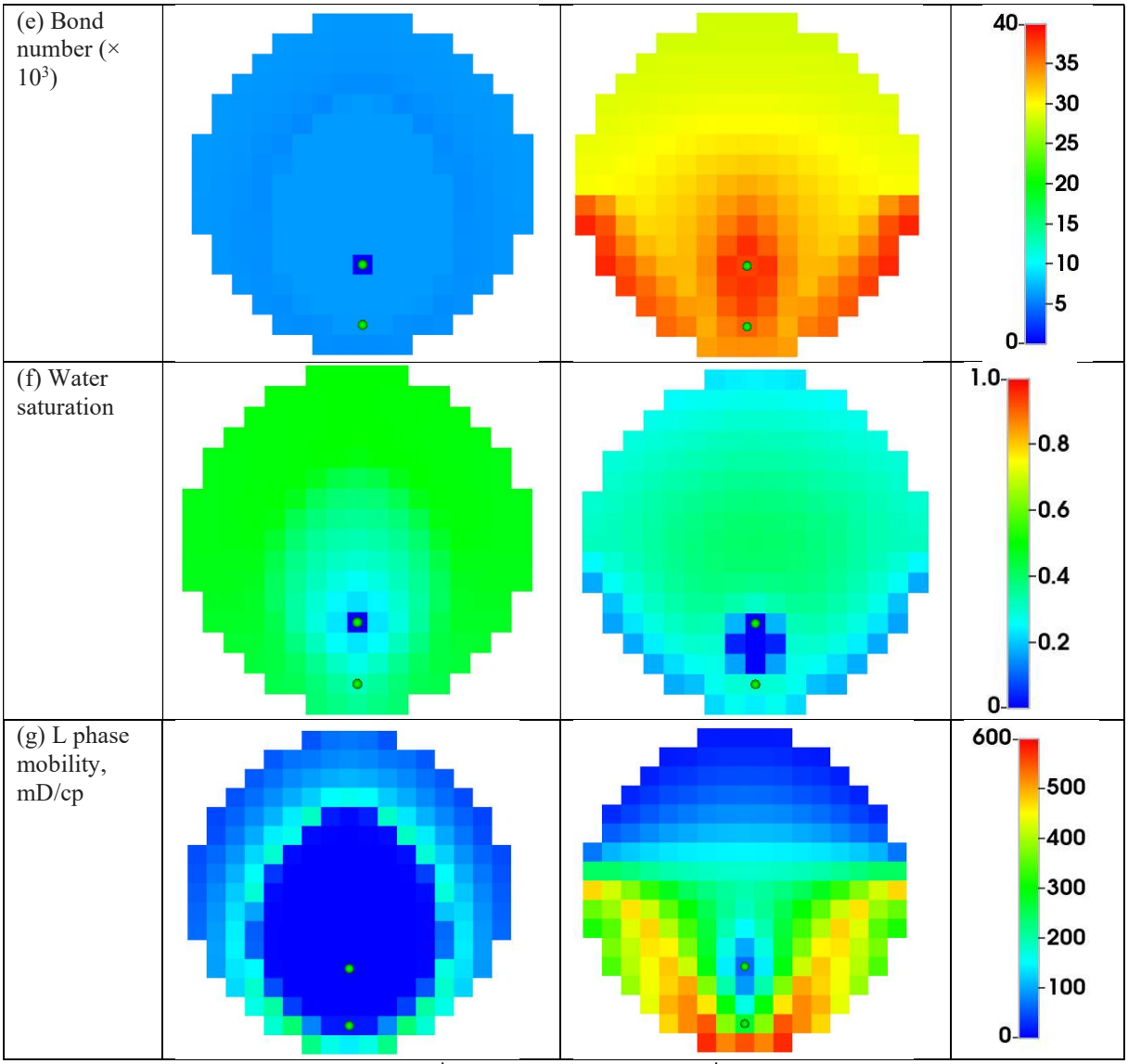

Fig. 18—2-D maps at Plane 4 for the SAGD (2nd column) and DME-SAGD (3rd column) experiments based on the calibrated numerical model at a bitumen recovery factor of 60%.

Conclusions

This paper presented an experimental program that used a large physical model to study the energy efficiency of DME-SAGD in comparison to SAGD. The sand pack used was 0.425 m in diameter and 1.22 m in length with an average porosity of 0.33 and a permeability of 5 D. Two experiments, SAGD and 10 mol% DME-SAGD, were performed at 3,000 kPa. The experimental data (compositional material balance and temperature distributions) were history-matched by a numerical simulation model. The main conclusions are as follows:

1. The cumulative steam-oil ratio for the DME-SAGD experiment was less than half of that for SAGD. The DME-SAGD experiment reached a bitumen recovery factor (RF) of 92.7% in 4.2 days, and the SAGD experiment reached a RF of 68.6% in 6 days. For both, the first two days were the preheating and steam-only injection stages (without DME). The increased rate of bitumen production contributed to the energy efficiency of DME-SAGD.
2. Analysis of the experimental data indicated that the mutual solubility of DME in the L and W phases resulted in flow characteristics in DME-SAGD that were different from those in SAGD. For example, the L and W phases were more uniformly distributed in the sand pack in the DME-SAGD experiment than in the SAGD experiment. The enhanced bitumen production by DME-SAGD was confirmed by a distribution of greater grid-scale Bond numbers and increased L-phase mobilities; for instance, the DME-SAGD experiment exhibited a grid-scale Bond number that was an order of magnitude greater than that of SAGD.
3. Lowering IFTs was necessary to match the 10 mol% DME-SAGD experimental data, particularly temperature distributions. This was expected from the partitioning of DME into the three phases and consistent with the previous DME-steam soaking experiment of bitumen gravity drainage (Amer et al. 2024b).

Nomenclature

ρ	Density, kg/m^3
ω	Acentric factor
λ	Phase mobility, D/cp
ϕ	Porosity
σ	Interfacial tension, dynes/cm
E_{in}	Cumulative energy input, kJ
$E_{in}-E_{out}$	Cumulative net energy, kJ
r	Diameter of pore size, μm

Acknowledgements

We thank ConocoPhillips for the financial support and permission for this publication. We also thank the sponsors of the Energi Simulation Industrial Affiliate Program on Carbon Utilization and Storage (ES Carbon UT) at the University of Texas at Austin. Ryosuke Okuno holds the Pioneer Corporation Faculty Fellowship in Petroleum Engineering at the University of Texas at Austin.

References

Amer, H., Sheng, K., Okuno, R. et al. 2024a. A Systematic Comparison Of Solvents And Their Concentrations In Bitumen Gravity Drainage Under Controlled Thermodynamic Conditions. *Fuel* **357** (A): p.129723. https://doi.org/10.1016/j.fuel.2023.129723.

Amer, H., Sheng, K., Okuno, R. et al. 2024b. Gravity Drainage Of Bitumen Under Controlled Thermodynamic Conditions In DME-Steam Co-Injection. *Geoenergy Science and Engineering* **233**: p.212539. https://doi.org/10.1016/j.geoen.2023.212539.

Baek K. H., Sheng K., Arguelles-Vivas F. J. et al. 2019. Comparative Study Of Oil-Dilution Capability Of Dimethyl Ether And Hexane As Steam Additives For Steam-Assisted Gravity Drainage. *SPE Res Eval & Eng* **22**(3): 1030-48. SPE-187182-PA. https://doi.org/10.2118/187182-PA.

Bentsen, R. G. and Manai, A. A. 1993. On The Use Of Conventional Cocurrent And Countercurrent Effective Permeabilities To Estimate The Four Generalized Permeability Coefficients Which Arise In Coupled, Two-Phase Flow. *Transport Porous Media* **11** (3): 243–262. https://doi.org/10.1007/ BF00614814.

Bourbiaux, B. J. and Kalaydjian, F. J. 1990. Experimental Study of Cocurrent and Countercurrent Flows in Natural Porous Media. *SPE Res Eval & Eng* **5** (3): 361–368. SPE-18283-PA. https://doi.org/10.2118/18283-PA.

Butler, R. M. 1985. A New Approach to The Modelling of Steam-Assisted Gravity Drainage. *J. Can. Petrol. Technol.* **24** (03): 42–51. https://doi.org/10.2118/85-03-01.

Cai H., Brandt A. R., Yeh S. et al. 2015. Well-to-wheels greenhouse gas emissions of Canadian Oil Sands Products: Implications for U.S. petroleum fuels. *Environ Sci Tech* **49** (13):8219–27. https://doi/10.1021/acs.est.5b01255.

Chai, M., Chen, Z., Nourozieh, H. et al. 2023. Introduce Dimethyl Ether (DME) As A Solvent For Steam-Assisted Gravity Drainage (SAGD) Co-Injection: An Effective And Environmental Application. *Fuel* **341**: p.127639. https://doi.org/10.1016/j.fuel.2023.127639.

Chai, M., Yang, M., and Chen, Z. 2022. Systematical Study On Dimethyl Ether As A Renewable Solvent For Warm Vapex And Its Significant Implications For The Heavy Oil Industry. *Fuel*, **312**: p.122911. https://doi.org/10.1016/j.fuel.2021.12291.

Chernetsky, A., Masalmeh, S., Eikmans, D. et al. 2015. A Novel Enhanced Oil Recovery Technique: Experimental Results and Modelling Workflow of the DME Enhanced Waterflood Technology. Presented at the Abu Dhabi International Petroleum Exhibition and Conference, Abu Dhabi, 9–12 November. SPE-177919-MS. https://doi.org/10.2118/177919-MS.

Computer Modelling Group. 2023. STARS Version 2023 User's Guide. Calgary, Alberta, Canada: Computer Modelling Group.

deFernández M. E. P., Calado J. C. G., Zollweg J. A. et al. 1992. Vapor-liquid equilibria in the binary system dimethyl ether + n-butane from 282.9 to 414.5 K at pressures to 4.82 MPa. *Fluid Phase Equilibria* **74**: 289–302. https://doi.org/10.1016/0378-3812(92)85068-J.

Gates, I. D., and Larter, S. R. 2014. Energy Efficiency And Emissions Intensity Of SAGD. *Fuel* **115**: 706-13. https://doi.org/10.1016/j.fuel.2013.07.073.

Haddadnia, A., Zirrahi, M., Hassanzadeh, H. et al. 2018a. Dimethylether-A Promising Solvent for ES-SAGD. Presented at the SPE Canada Heavy Oil Technical Conference, Calgary, Alberta, Canada, 13–14March. SPE-189741-MS. https://doi.org/10.2118/189741-MS.

Haddadnia, A., Azinfar, B., Zirrahi, M. et al. 2018b. Thermophysical Properties Of Dimethyl Ether/Athabasca Bitumen System. *The Canadian Journal of Chemical Engineering* **96** (2): 597-604. https://doi.org/10.1002/cjce.23009.

Holldorff, H. and Knapp, H. 1988. Binary Vapor-Liquid-Liquid Equilibrium of Dimethyl Ether—Water and Mutual Solubilities of Methyl Chloride and Water. *Fluid Phase Equilibria* **44** (2): 195–209. https://doi.org/10.1016/0378-3812(88)80111-0.

Huron, M. J. and Vidal, J. 1979. New Mixing Rules in Simple Equations of State for Representing Vapour-Liquid Equilibria of Strongly Non-ideal Mixtures. *Fluid Phase Equilibria* **3** (4): 255–271. https://doi.org/10.1016/0378-3812(79)80001-1.

Javanmard, H., Seyyedi, M., Jones, S.A. et al. 2019. Dimethyl Ether Enhanced Oil Recovery In Fractured Reservoirs And Aspects Of Phase Behavior. *Energy & Fuels* **33**: 10718–10727. https://doi.org/10.1021/acs.energyfuels.9b02600.

Kalaydjian, F. 1990. Origin and Quantification of Coupling between Relative Permeabilities for Two-Phase Flows in Porous Media. *Transport Porous Media* **5** (3): 215–229. https://doi.org/10.1007/BF00140013.

Keshavarz, M., Okuno, R., and Babadagli, T. 2015. Optimal Application Conditions for Steam-Solvent Coinjection. *SPE Res Eval & Eng* **18** (1): 20-38. SPE-165471-PA. https://dx.doi.org/10.2118/165471-PA.

Kumar, A., and Okuno, R., 2016. A New Algorithm For Multiphase-Fluid Characterization For Solvent Injection. *SPE J* **21** (5): 1688–1704. SPE-175123-PA. https://doi.org/10.2118/175123-PA.

Lee, Y. W., Lee, H. S., Jeong, M. S. et al. 2021. Compositional Modeling Of Dimethyl Ether–CO_2 Mixed Solvent For Enhanced Oil Recovery. *Applied Sciences* **11**(1): 406. https://doi.org/10.3390/app11010406.

Li, S., Peng, D., Feng, S. et al. 2023. Dimethyl Ether-Steam Assisted Gravity Drainage: Physical 2D Heavy Oil Simulation. *Fuel* **342**: p.127821. https://doi.org/10.1016/j.fuel.2023.127821.

Mahdizadeh, M., Eftekhari, A. A., and Nick, H. M. 2019. Numerical Modeling Of Water-Soluble Solvents For Enhancing Oil Recovery In Heterogeneous Chalk Reservoirs. *J Petrol Sci Eng* **175**:681–92. https://doi.org/10.1016/j.petrol.2018.12.083.

Nasr, T. N., Law, D. H. S., Golbeck, H. et al. 2000. Counter-Current Aspect Of The SAGD Process. *Journal of Canadian Petroleum Technology* **39** (01). https://doi.org/10.2118/00-01-03.

Nasr, T. N., Beaulieu, G., Golbeck, H. et al. 2003. Novel Expanding Solvent-SAGD Process "ES-SAGD." *Journal of Canadian Petroleum Technolog* **42**(01): 13–16. https://doi.org/10.2118/03-01-TN.

Ng, K.L., Chadwick, D., and Toseland, B. A. 1999. Kinetics And Modelling Of Dimethyl Ether Synthesis From Synthesis Gas. *Chemical Engineering Science* **54**(15-16): 3587-92. https://doi.org/10.1016/S0009-2509(98)00514-4.

Okuno, R. 2018. "Coinjection of Dimethyl Ether and Steam for Bitumen and Heavy Oil Recovery," Patent No.: 10,125,591 B2. http://dx.doi.org/10.26153/tsw/3613.

Ovalles, C. 2019. Subsurface Upgrading of Heavy Crude Oils and Bitumen. Boca Raton, Florida, USA: CRC Press.

Parsons, C., Chernetsky, A., Eikmans, D. et al. 2016. Introducing a Novel Enhanced Oil Recovery Technology. Presented at the SPE Improved Oil Recovery Conference, Tulsa, 11 13 April. SPE-179560-MS. https://doi.org/10.2118/179560-MS.

Pozo, M. E. and Streett, W. B. 1984. Fluid Phase Equilibria for the System Dimethyl Ether/Water from 50 to 220°C and Pressures to 50.9 MPa. *J. Chem. Eng. Data* **29** (3): 324–329. https://doi.org/10.1021/je00037a030.

Pratama, R. A. and Babadagli, T. 2020. Reconsideration Of Steam Additives To Improve Heavy-Oil Recovery Efficiency: Can New Generation Chemicals Be A Solution For Steam-Induced Unfavorable Wettability Alteration?. *Energy & Fuels* **34** (7): 8283-8300. https://doi.org/10.1021/acs.energyfuels.0c01406.

Pratama, R. A. and Babadagli, T. 2021. Tertiary-Recovery Improvement of Steam Injection Using Chemical Additives: Pore-Scale Understanding of Challenges and Solutions Through Visual Experiments. *SPE J* **26**: 1552–1571. https://doi.org/10.2118/200841-PA.

Ratnakar, R. R., Dindoruk, B., and Wilson, L. 2016a. Experimental Investigation of DME-Water-Crude Oil Phase Behavior and PVT Modeling for the Application of DME-Enhanced Waterflooding. *Fuel* **182**: 188–197. https://doi.org/10.1016/j.fuel.2016.05.096.

Ratnakar, R. R., Dindoruk, B., and Wilson, L. 2016b. Phase Behavior Experiments and PVT Modeling of DME-Brine-Crude Oil Mixtures Based on Huron-Vidal Mixing Rules for EOR Applications. *Fluid Phase Equilibria* **434**: 49–62. https://doi.org/10.1016/j.fluid.2016.11.021.

Robinson, D. B. and Peng, D. Y. 1978. The Characterization of the Heptanes and Heavier Fractions for the GPA Peng-Robinson Programs. *Research Report RR-28*, Gas Processors Association, Tulsa.

Sheng, K., Okuno, R., and Wang, M. 2017. Water-Soluble Solvent as an Additive to Steam for Improved SAGD, Presented at SPE Canada Heavy Oil Technical Conference, February 15 – 16, Calgary, Alberta, Canada. SPE-184983-MS. https://doi.org/10.2118/184983-MS.

Sheng, K., Okuno, R., and Wang, M. 2018. Dimethyl Ether as an Additive to Steam for Improved Steam-Assisted Gravity Drainage. *SPE J* **23** (04): 1201–1222. SPE-184983-PA. https://doi.org/10.2118/184983-PA.

Sheng, K., Okuno, R., Imran, M. et al. 2021. An Experimental Study of Steam-Assisted Gravity Drainage. *SPE J* **26**: 1515–1534. SPE-200867-PA. https://doi.org/10.2118/200867-PA.

Sheng, K., Amer, H., Liu, Y. et al. 2022a. A New Experimental Method For Comparing Solvents In Steam-Solvent Coinjection For Bitumen Recovery Under Controlled Thermodynamic Conditions. *Journal of Petroleum Science and Engineering* **213**: 110377. https://doi.org/10.1016/j.petrol.2022.110377.

Sheng, K., Okuno, R., Al-Gawfi A. et al. 2022b. An Experimental Study of Steam-Solvent Coinjection for Bitumen Recovery Using a Large-Scale Physical Model. *SPE J* **27**(01): 381–398. SPE-205158-PA. https://doi.org/10.2118/205158-PA.

Sheng, K., Okuno, R., Al-Gawfi, A. et al. 2023. The Impact Of Permeability Barriers On Steam-Solvent Coinjection–A Mechanistic Study Using A Physical Model. *Geoenergy Science and Engineering* **223**, p.211569. https://doi.org/10.1016/j.geoen.2023.211569.

Soave, G. 1972. Equilibrium Constants From a Modified Redlich-Kwong Equation of State. *Chem. Eng. Sci.* **27** (6): 1197–1203. https://doi.org/10.1016/0009-2509(72)80096-4.

Stewart, R. A., and Shaw, J. M. 2018. Interface Renewal and Concentration Shock Through Sloughing: Accounting for the Dissonance Between Production Models and Measured Outcomes for Solvent–Assisted Bitumen–Production Processes. *SPE Res Eval & Eng* **21**: 174–186. SPE-186108-PA. https://doi.org/10.2118/186108-PA.

Xu, M., Lunsford, J. H., Goodman, D. W. et al. 1997. Synthesis Of Dimethyl Ether (DME) From Methanol Over Solid-Acid Catalysts. *Applied Catalysis A: General* **149** (2): 289-301. https://doi.org/10.1016/S0926-860X(96)00275-X.

Yang, M., Chai, M., Qi, R. et al. 2021. Dimethyl Ether As A Novel Solvent For Bitumen Recovery: Mechanisms Of Improved Mass Transfer And Energy Efficiency. *SPE J* **27** (02): 1321–1340. SPE-208615-PA. https://doi.org/10.2118/208615-pa.

Zhao, X., Zhou, F., Chen, Z. et al. 2023. Dynamic Monitoring and Enhanced Oil Recovery Evaluation of the Water Flooding Process of Liquid Nanofluids in Tight Reservoirs. *Energy & Fuels* **37** (6): 4256-4266. https://doi.org/10.1021/acs.energyfuels.2c03936.

Zhu, D., and Okuno, R., 2014. A Robust Algorithm For Isenthalpic Flash Of Narrow-Boiling Fluids. *Fluid Phase Equilibria* **379**: 26-51. https://doi.org/10.1016/j.fluid.2014.07.003.

Appendix A—Adjusted Parameters for Calibrated Numerical Models

This appendix presents the adjusted heat loss and relative permeability parameters obtained after history-matching the SAGD and 10 mol% DME-SAGD experiments. The history-matching of SAGD encompassed two consecutive simulations: Period 1 (first 48 hours) and Period 2 (rest of SAGD). The history-matching of DME-SAGD was also performed for two stages: steam and DME/steam. To model the varying operation conditions of band heaters at each period (or stage), the sand pack within the numerical model was segmented into five sections (**Figure A-1**). Each segment was then assigned specific heat loss parameters to match temperature and compositional material balance data. **Tables A-1 and A-2** summarize heat loss parameters for the two end flanges and the five sand pack segments during the aforementioned periods and stages for both SAGD and 10 mol% DME-SAGD calibrated numerical models. **Table A-3** summarizes the relative permeability curve parameters for SAGD and 10 mol% DME-SAGD.

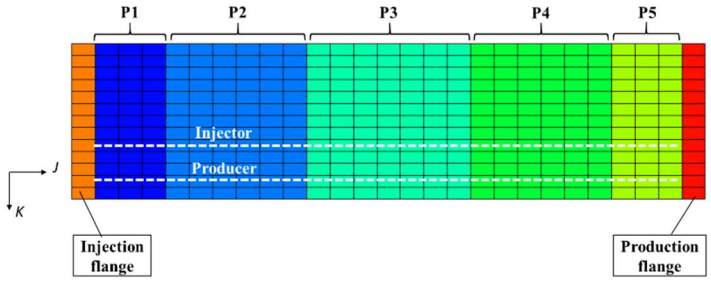

Fig. A-1—Longitudinal cross-section view of the simulation model in *J* and *K* directions. The sand pack within the numerical model was segmented into five sections (P1 through P5), in addition to the two end flanges.

	Injection-End Flange	Production-End Flange	P1	P2	P3	P4	P5
			(a) Period 1				
Heat conductivity in *I*, J/(m×day×°C)	-	-	14.4×10^3	14.4×10^3	6.0×10^3	14.4×10^3	14.4×10^3
Volumetric heat capacity in *I*, J/(m^3×°C)	-	-	2.0×10^6	2.0×10^6	5×10^5	2.0×10^7	2.0×10^7
Heat conductivity in *J*, J/(m×day×°C)	14.4×10^5	14.4×10^5	-	-	-	-	-
Volumetric heat capacity in *J*, J/(m^3×°C)	2.5×10^7	2.5×10^7	-	-	-	-	-
Heat conductivity in –*K*, J/(m×day×°C)	5.76×10^5	5.76×10^5	14.4×10^3	12.0×10^3	-	14.4×10^4	14.4×10^4
Volumetric heat capacity in –*K*, J/(m^3×°C)	2.0×10^6	2.0×10^6	2.0×10^6	2.0×10^6	-	10×10^7	10×10^7
			(b) Period 2				
Heat conductivity in *I*, J/(m×day×°C)	-	-	1.0×10^5	1.0×10^5	1.0×10^5	1.0×10^5	1.0×10^5
Volumetric heat capacity in *I*, J/(m^3×°C)	-	-	2.0×10^7	2.0×10^7	2.0×10^7	2.0×10^7	2.0×10^7
Heat conductivity in *J*, J/(m×day×°C)	14.4×10^5	14.4×10^5	-	-	-	-	-
Volumetric heat capacity in *J*, J/(m^3×°C)	2.5×10^7	2.5×10^7	-	-	-	-	-
Heat conductivity in –*K*, J/(m×day×°C)	5.76×10^5	5.76×10^5	1.0×10^4	1.0×10^4	1.0×10^4	1.0×10^4	1.0×10^4
Volumetric heat capacity in –*K*, J/(m^3×°C)	2.0×10^6	2.0×10^6	2.0×10^5	2.0×10^5	2.0×10^5	2.0×10^5	2.0×10^5

Table A-1—Adjusted heat loss parameters for Periods 1 and 2 after history matching SAGD experiment. *I*, *J*, and –*K* are the directions perpendicular to the well pair, along the well pair, and overburden, respectively.

	Injection-End Flange	Production-End Flange	P1	P2	P3	P4	P5
			(a) SAGD stage				
Heat conductivity in *J*, J/(m×day×°C)	14.4×10^5	14.4×10^5	-	-	-	-	-
Volumetric heat capacity in *J*, J/(m^3×°C)	2.5×10^7	2.5×10^7	-	-	-	-	-
Heat conductivity in *–K*, J/(m×day×°C)	14.4×10^5	14.4×10^5	14.4×10^3	14.4×10^2	14.4×10^2	14.4×10^2	14.4×10^3
Volumetric heat capacity in *–K*, J/(m^3×°C)	2.5×10^7	2.5×10^7	2.0×10^6	2.0×10^5	2.0×10^5	2.0×10^6	2.0×10^6
Heat conductivity in *+K*, J/(m×day×°C)	5.76×10^5	5.76×10^5	14.4×10^3	14.4×10^2	14.4×10^2	14.4×10^2	14.4×10^3
Volumetric heat capacity in *+K*, J/(m^3×°C)	2.0×10^6	2.0×10^6	2.0×10^6	2.0×10^5	2.0×10^5	2.0×10^6	2.0×10^6
			(b) DME/steam stage				
Heat conductivity in *J*, J/(m×day×°C)	14.4×10^5	14.4×10^5	-	-	-	-	-
Volumetric heat capacity in *J*, J/(m^3×°C)	2.5×10^7	2.5×10^7	-	-	-	-	-
Heat conductivity in *–K*, J/(m×day×°C)	5.76×10^5	5.76×10^5	14.4×10^3	14.4×10^3	14.4×10^3	14.4×10^3	14.4×10^3
Volumetric heat capacity in *–K*, J/(m^3×°C)	2.0×10^6	2.0×10^6	2.0×10^6	2.0×10^6	2.0×10^6	2.0×10^6	2.0×10^6
Heat conductivity in *+K*, J/(m×day×°C)	5.76×10^5	5.76×10^5	14.4×10^3	14.4×10^3	14.4×10^3	14.4×10^3	14.4×10^3
Volumetric heat capacity in *+K*, J/(m^3×°C)	2.0×10^6	2.0×10^6	2.0×10^6	2.0×10^6	2.0×10^6	2.0×10^6	2.0×10^6

Table A-2—Adjusted heat loss parameters for SAGD and DME/steam stages after history matching the 10 mol% DME-SAGD experiment. *I*, *J*,*–K,* and *+K* are the directions perpendicular to the well pair, along the well pair, and over- and underburden, respectively.

Model parameters	Period 1 (SAGD)	Period 2 (SAGD)	DME/steam
S_{wr}	0.08	0.08	0.22
S_{or} (oil/water, oil/gas)	0.25	0.20	0.07
S_{gr}	0	0	0
K_{ro} ($S_w = S_{wr}$)	0.30	0.70	0.75
K_{rw} ($S_w = 1–S_{or}$)	0.50	0.05	0.05
K_{rg} ($S_l = 1–S_{gr}$)	0.30	0.30	0.80

Table A-3— Relative permeability endpoints and residual saturations for the three-phase Stone I model after history-matching the SAGD and the 10 mol% DME-SAGD experiments.

Appendix B—Results of Dean-Stark analysis performed on samples taken from the sand pack

This appendix presents Dean-Stark analysis results and asphaltene weight% for the sand samples taken from the excavated sand pack for the SAGD (**Table B1**) and the 10 mol% DME-SAGD (**Table B2**) experiments. Overall, DME-SAGD resulted in lower remaining oil saturations than SAGD, indicating enhanced bitumen drainage. The asphaltene content within the sand samples was determined using a solvent extraction process similar to Amer et al. (2024a). Normal-pentane (n-C_5) was added to the remaining oil, which was extracted from the sand samples using the Dean Stark method. This resulted in precipitation of the asphaltene components as solid particles. Then, the precipitated asphaltene components were removed from the solution by filtration, and their weight was measured. The mass of the asphaltene precipitation was divided by the mass of the remaining oil to calculate the asphaltene weight percent in the remaining oil.

Sample #	Oil saturation (%)	Water saturation (%)	Gas saturation (%)	Asphaltene wt% in the remaining oil
		Injection End		
1	15.8	10.5	73.7	17.7
4	36.5	15.6	47.9	23.5
5	90.2	8.8	1.1	18.6
7	7.6	19.9	72.4	24.3
8	22.0	24.0	54.0	17.9
9	19.4	32.9	47.6	18.2
11	6.0	17.0	77.0	7.0
12	16.4	9.9	73.7	20.4
14	35.1	22.2	42.7	23.1
15	69.1	12.8	18.2	18.6
16	15.1	6.0	78.9	20.4
19	23.1	22.9	54.0	21.2
20	16.6	37.1	46.3	20.6
21	10.9	13.2	76.0	20.4
23	13.5	30.2	56.3	20.1
24	10.1	32.4	57.5	25.2
		Production End		
26	8.7	17.1	74.2	14.6
28	21.6	27.6	50.8	20.2
30	82.6	6.2	11.2	18.7
32	27.4	12.4	60.2	21.8
33	42.6	6.3	51.1	19.0
34	14.2	35.1	50.7	17.8
36	13.0	8.8	78.3	20.4
37	9.7	12.6	77.7	13.9
38	9.5	28.2	62.4	25.0
40	64.4	24.6	11.0	17.7

Table B-1—Dean-Stark analysis results and asphaltene weight% for the samples taken from the excavated sand pack of the SAGD experiment.

Sample #	Oil saturation (%)	Water saturation (%)	Gas saturation (%)	Asphaltene wt% in the remaining oil
		Injection End		
22	12.5	1.1	86.4	21.7
23	20.9	1.1	78.0	22.8
25	18.1	1.1	80.8	21.3
26	10.2	1.1	88.7	20.0
28	13.0	0.5	86.5	27.4
29	10.8	1.1	88.1	20.5
31	10.3	1.6	88.1	19.4
33	9.7	1.6	88.7	27.7
34	58.1	0.6	41.3	24.5
35	19.8	1.1	79.1	21.6
36	13.0	1.6	85.3	20.8
37	11.4	1.6	87.0	20.4
39	18.1	1.7	80.3	23.6
		Production End		
1	11.3	0.5	88.1	22.1
3	14.1	1.1	84.8	22.0
5	50.4	0.6	49.0	22.4
6	11.3	0.5	88.1	21.4
8	10.2	1.1	88.7	21.6
10	58.1	0.6	41.3	21.9
11	11.4	1.1	87.6	19.4
13	12.5	1.1	86.4	20.0
14	17.5	1.1	81.4	22.0
15	29.6	1.1	69.2	21.0
17	10.8	1.1	88.1	21.0
19	13.6	1.1	85.3	19.8
20	38.6	0.6	60.9	22.3

Table B-2—Dean-Stark analysis results and asphaltene weight% for the samples taken from the excavated sand pack of the 10 mol% DME-SAGD experiment.